nucleotides and the amino acids of the protein, were numbered based on the GenBank sequence information (accession no. NM_000445.3). PCR amplification of two parts of exon 32 was performed using the following primers. Primers 5'-GTGGAGACCACGCAGGTGTAC-3' and 5'-GGAGCCCGTGCCATAGAGG-3' for a single part of exon 32 synthesized a 420-bp fragment including c.10735 to c.11154. Primers 5'-AGCGGCTGACTGTGGATGAGG-3' and 5'-TGCGTGTCCTTGTTGAGGT-3' for another single part of exon 32 synthesized a 283-bp fragment including c.11230 to c.11512. Both of the mutations in the proband were confirmed by restriction digestion of PCR products. c.10984C>T and c.11453_11462del caused the generation of new restriction enzyme sites for *BsrI* and *BbvCI*, respectively.

The mutation nomenclature follows the journal's guidelines (www.hgvs.org/mutnomen) according to the reference sequence NM_000445.3, with +1 as the A of the ATG initiation codon.

Haplotype analysis

Genotype analysis of this family to establish the *de novo* nature of c.11453_11463del in the proband was performed using three chromosome 8 markers (D8S272, D8S264, D8S270) and six non-chromosome 8 markers (D1S468, D1S252, D1S2842, D3S1297, D3S1566 and D3S1311). All microsatellite markers (ABI Prism Linkage Mapping Set Version 2.5; Applied Biosystems, Warrington, UK) were amplified with fluorescently labeled oligonucleotides and used under conditions recommended by the manufacturer. Electrophoretic analysis was performed on an ABI Prism 310 Genetic Analyzer with Performance Optimized Polymer 4 (POP4) using GeneScan software (Applied Biosystems). The allele sizes were analyzed using Genotyper software (Applied Biosystems).

Immunofluorescence Studies

Immunofluorescence analysis was performed using skin specimens from the proband as previously described (Natsuga, et al., 2010). Briefly, fresh-frozen skin specimens were embedded in optimal cutting temperature (OCT) compound and quickly frozen in isopentane cooled over liquid nitrogen. 5-μm cryostat sections were incubated with primary antibodies. After washing in phosphate-buffered saline, the sections were incubated with secondary antibodies conjugated with fluorescein-isothiocyanate.

Antibodies

The following antibodies against basement membrane zone (BMZ) components were used: monoclonal antibody (mAb) PN643 against the N-terminal actin-binding domain of plectin; mAb HD1-121 against the rod domain of plectin; C20 and mAb PC-815 against the C-terminal globular domain of plectin (Fig. 1A); mAbs GoH3 and 3E1 (Chemicon International, CA) against α6 and ß4 integrins, respectively; mAb GB3 (Sera-lab, Cambridge, UK) against laminin 332; mAb LH7.2 (Sigma, St. Louis, MO) against type VII collagen; mAb PHM-12^{+}CIV22 against type IV collagen (NeoMarkers, Fremont, CA); and S1193 and mAb HDD20 against BP230 and type XVII collagen, respectively. mAbs PN643, HD1-121 and PC815 were generously donated by Prof. K. Owaribe of Nagoya University, and antibody S1193 by Prof. J. R. Stanley of the University of Pennsylvania. C20, a goat polyclonal antibody against the C-terminus of plectin, was purchased from Santa Cruz. Anti-beta-actin mAb (AC15, Sigma, St. Louis, MO) was used to confirm equal protein loading.

Cell Culture and Immunoblot Analysis

Cell culture and immunoblot analysis was performed as previously described (Natsuga, et al., 2010). Cultured fibroblasts were obtained from skin biopsies of a normal human volunteer and the proband. Cultured fibroblasts were maintained in Dulbecco's modified Eagle's medium supplemented with 10% (v/v) fetal bovine serum. For sample preparation, cultured cells were lysed in Nonidet-40 (NP-40) containing buffer (1% NP-40, 25mM Tris-HCl (pH 7.6), 4mM EDTA, 100mM NaCl, 1mM phenylmethylsulfonyl fluoride (PMSF), and proteinase inhibitor

cocktail (Sigma, St. Louis, MO)); cell debris was removed by centrifugation; and the supernatant was collected. Supernatants were boiled in Laemmli's sample buffer (Laemmli, 1970), applied to a 4–12% gradient Bis-Tris gel (Invitrogen, Carlsbad, CA), and transferred to a PVDF membrane. The membrane was incubated with PN643, HD1-121, C20 and AC15 followed by incubation with horseradish peroxidase (HRP) conjugated anti-mouse IgG (for PN643, HD1-121 and AC15) and HRP-conjugated anti-gout IgG (for C20). The blots were detected using ECL Plus Detection Kit (GE Healthcare, Fairfield, CT).

Semi-quantitative RT-PCR Analysis

Semi-quantitative reverse transcription PCR (RT-PCR) analysis was performed as previously described (Natsuga, et al., 2010). Total RNA was isolated from cultured fibroblasts (from normal human volunteers and the proband, using RNeasy kit (Qiagen, Valencia, CA)), and first-strand cDNA was made using Superscript III reverse transcriptase (Invitrogen, Carlsbad, CA). First-strand cDNA was then amplified by PCR with primers specific for the exon boundaries flanking the rod domain of plectin as described previously (Koster, et al., 2004; Natsuga, et al., 2010). The following primers were used (Fig. 1B): 30F, 5'-CATCAGCGAGACTCTGCGGC-3'; 31R, 5'-TGCGCCTGTCGCTTTTGTGC-3'; 31F, 5'-AGCTGGAGATGAGCGCTGA-3'; 32R, 5'-TGCTGCAGCTCCTCCTGC-3'. To ensure equal loading, a housekeeping gene (GAPDH) was simultaneously amplified. The PCR products were assessed on a 2% agarose gel. The images were obtained with LAS-4000 mini (Fujifilm, Tokyo, Japan).

The medical ethics committee of Hokkaido University Graduate School of Medicine approved all of the described studies. The study was conducted according to The Declaration of Helsinki Principles. Participants gave their written informed consent.

RESULTS

Case Description

The proband was a first child of non-consanguineous Japanese parents. There was no family history of bullous diseases. He was born by cesarean section after a 39-week gestation because of non-reassuring fetal status. Clinically the proband showed extensive blistering and aplasia cutis on the extremities (Fig. 2A, B). Routine abdominal X-ray revealed a single bubble sign, suggesting the presence of PA (Fig. 2C). Generalized muscle hypotonia, dysphagia and difficulty in breathing were also observed from birth. Laboratory examination at birth revealed markedly elevated levels of creatine kinase (CK) (11,852U/L, normal value; 60-400U/L). The skeletal muscle isoform of CK (CK-MM) was 84% of total CK (CK, 2058U/L at age 12 days). Elevated levels of muscle enzymes including CK and aldolase (normal value; 1.7-5.7U/L) persisted over the course of his life (CK, 1924U/L; aldolase, 40.0U/L at age 25 days). Based on the clinical features and laboratory data, the presence of MD was confirmed. Muscle biopsy and reconstructive surgery for PA was not performed because the parents did not consent. The proband died 3 months after birth. Permission for autopsy was refused.

Skin Separation in Basal Keratinocytes

Electron microscopy of the skin samples from the proband showed that the skin separation localized to the base of the basal keratinocytes (Fig. 2D). Hemidesmosomes were hypoplastic and found at the base of the intraepidermal split (Fig. 2D). Keratin clumps were not observed.

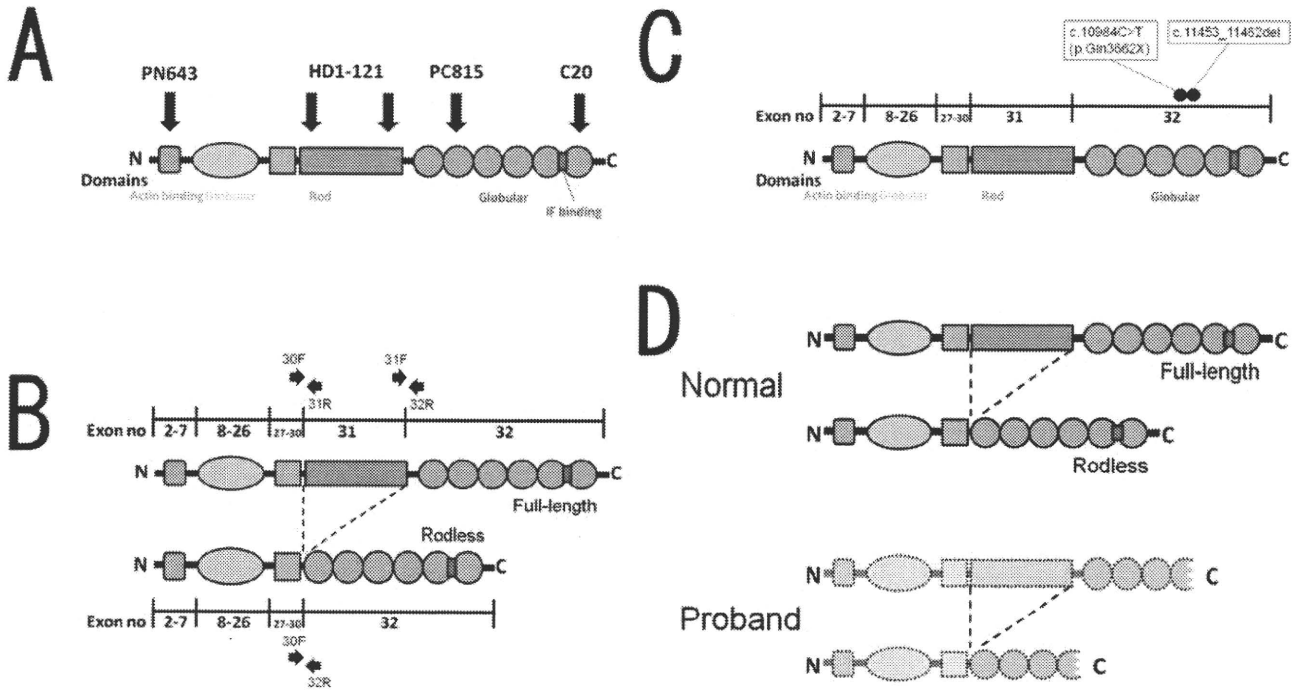

Figure 1. Plectin structure, antibodies against plectin, specific primers to amplify the full-length and the rodless plectin transcripts and *PLEC* mutations of the proband. (A) Plectin protein is composed of an actin-binding domain, N- and C-terminal globular domains, an intermediate filament (IF)-binding domain and a central rod domain. The C-terminal globular domain has 6 plectin repeat domains. The IF-binding domain is located between C-terminal repeats 5 and 6. PN643 is a monoclonal antibody (mAb) against the N-terminal actin-binding domain of plectin. HD1-121 is a mAb against the rod domain of plectin. PC815 is a mAb and C20 is a polyclonal antibody against the C-terminal globular domain of plectin. (B) The specific primers used to detect the presence of transcripts for full-length (30F/31R and 31F/32R) and rodless plectin (30F/32R) on cDNA synthesized from mRNA of normal humans and the proband's fibroblasts. (C) c.10984C>T and c.11453_11462del are located in the *PLEC* encoding C-terminal plectin repeat 4. (D) Normal humans express both full-length and rodless plectin. In our case, the *PLEC* mutations produced diminished and truncated plectin protein without the IF-binding domain.

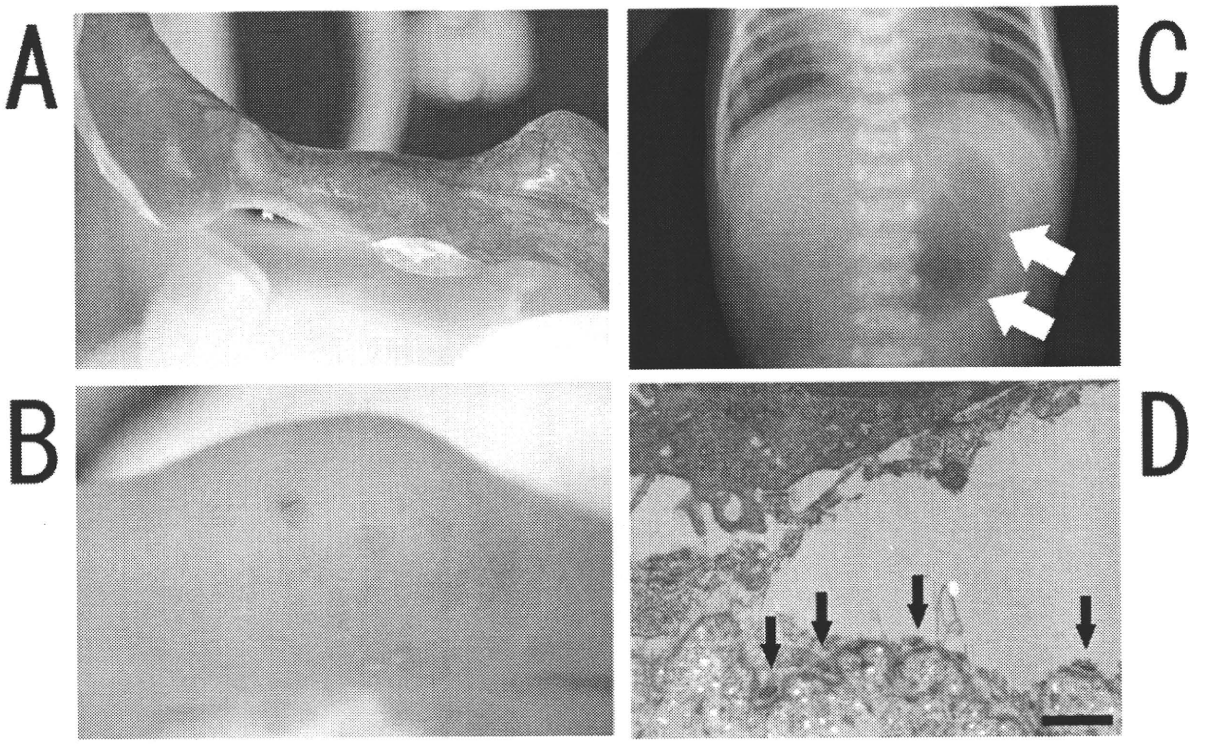

Figure 2. Clinical and ultrastructural features of the proband. (A) Aplasia cutis is observed on the left lower leg at birth. (B) Vesicles and erosions are scattered on the right knee. (C) Abdominal X-ray reveal single bubble sign (arrows), which indicated pyloric atresia. (D) Electron microscopy of the skin specimens from the proband reveals skin detachment within basal keratinocytes. Hemidesmosomes are hypoplastic and are observed at the base of the blisters (arrows) (Bar=1μm).

PLEC Mutations in Exon 32

PLEC mutational analysis demonstrated that the proband was compound heterozygous for maternal c.10984C>T (p.Glu3662X) and de novo c.11453_11462del in exon 32, the last exon of *PLEC* (Fig. 3A, 3B, 1C). The latter mutation is predicted to result in a frameshift that causes 88-amino-acid missense sequences followed by a premature termination codon (PTC). Both of the mutations were novel. c.10984C>T was confirmed by *BsrI* restriction enzyme digestion (Fig. 3C). c.11453_11462del was also confirmed by *BbvCI* restriction enzyme digestion (Fig. 3D) and TA-cloning (data not shown). Haplotype analysis of this family using microsatellite markers excluded false paternity as well as false maternity (data not shown) to establish the de novo nature of c.11453_11463del. The father's sperm has not been tested, although it might be beneficial to exclude the small possibility of paternal germ-line mosaicism through analyzing the father's sperm for any future prenatal diagnosis. In addition, c.7587G>A (p. =) transition in exon 32 was also detected in one allele of the proband and his father. This c.7587G>A transition was found in 3 of 100 normal unrelated alleles (50 healthy Japanese individuals), and was likely a polymorphism.

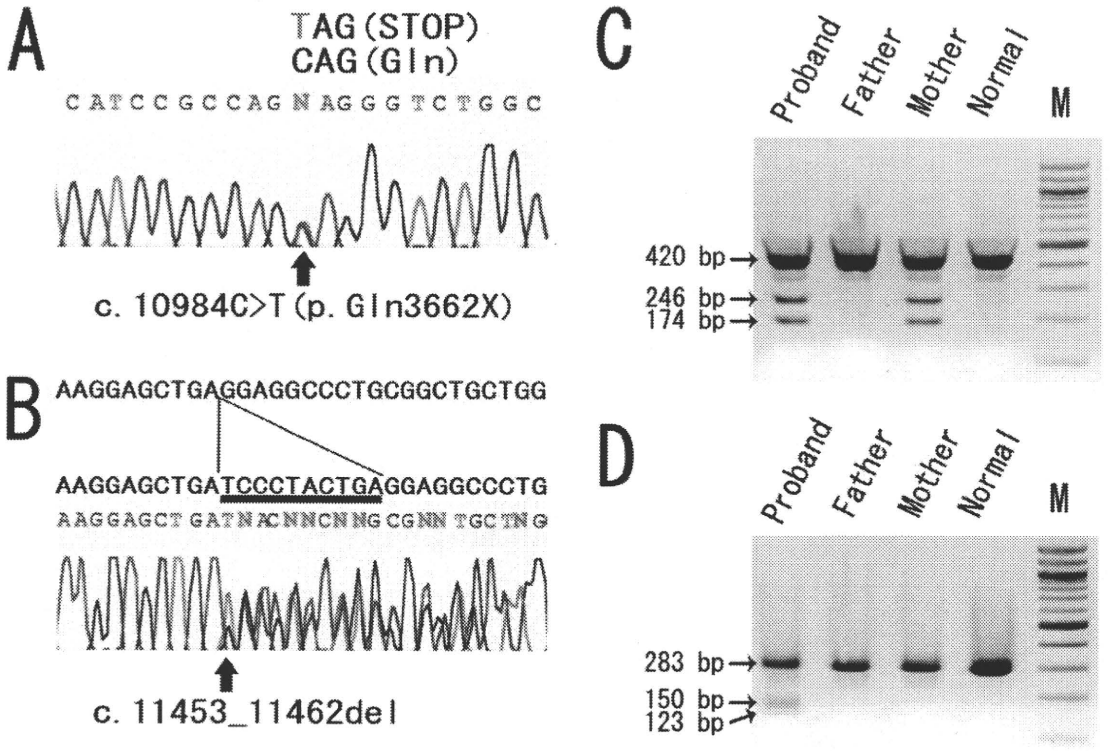

Figure 3. The novel *PLEC* mutations detected in the study. Maternal c.10984C>T (p.Gln3662X) (A) and de novo c.11453_11462del (B) in exon 32 were found in genomic DNA derived from the proband. A thymine substituted for a cytosine in the former mutation is indicated by the red character (A). Deleted nucleotides in the latter mutation are underlined (B). (C) c.10984C>T mutation caused the generation of a site for *BsrI* restriction enzyme. *BsrI* digestion of the 420-bp PCR product with and without the mutation resulted in a single band of 420-bp and in double bands of 246-bp and 174-bp, respectively. c.10984C>T was a maternal mutation. (D) c.11453_11462del caused the generation of a site for *BbvCI*. The 283-bp PCR product without the mutation was not digested by *BbvCI*. *BbvCI* digestion of the 273-bp PCR product with the deletion mutation showed two bands of 150 and 123-bp. c.11453_11462del was not detected in the parents' gDNA.

Diminished and Truncated Plectin Expression in Skin

We performed immunofluorescence analysis of the skin specimens from the proband using several antibodies that react with molecules of the dermo-epidermal junction (DEJ). To check plectin expression patterns in the skin specimens from the proband, we used four antibodies: PN643 (N-terminal globular domain), HD1-121 (rod domain), PC815 (C-terminal globular domain) and C20 (C-terminal globular domain) (Fig. 1A). Normal human control shows bright DEJ staining of all the antibodies tested (Fig. 4F-I). DEJ labeling of PN643, HD1-121 and PC815 was markedly diminished in the skin specimens from the proband (Fig. 4A-C). Staining of C20 was absent in the proband's skin (Fig. 4D). Immunostaining for type VII collagen (Fig. 4E), laminin 332, type IV collagen, type XVII collagen, α6 and β4 integrin, and BP230 revealed normal DEJ labeling patterns (data not shown).

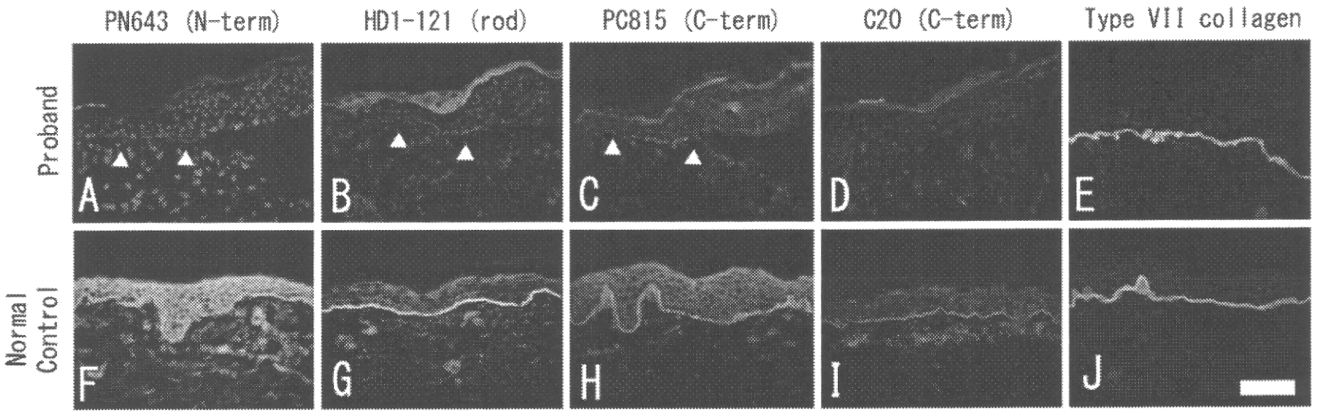

Figure 4. Immunofluorescence analysis of the proband's skin sample. In normal human skin, immunofluorescence shows that all of the antibodies against plectin (PN643, HD1-121, PC815 and C20) tested in this study bound to the dermal epidermal junction (DEJ) (F - I). DEJ labeling of PN643, HD1-121 and PC815 are weakly positive in the proband (A - C). In contrast, staining with C20 is negative in the proband's skin sample (D). Type VII collagen shows normal linear labeling in the proband and in the normal control (E, J). Weak labeling is indicated by arrowheads (Bar=100μm).

Diminished and Truncated Plectin in Cultured Fibroblasts

Immunoblot analysis of lysates from normal human cultured fibroblasts revealed that two closely spaced bands, corresponding to two forms of plectin (500kDa full-length and 390kDa rodless), reacted with PN643 and C20 antibodies recognizing the N- and C-termini of plectin (Fig. 5), as previously described (Natsuga, et al., 2010). HD1-121 against the rod domain reacted only with full-length plectin in normal human fibroblasts (Fig. 5). Lysates from cultured fibroblasts from the proband showed a faint band of PN643 and HD1-121 between 500kDa and 390kD, corresponding to truncated full-length plectin. C20 failed to react with lysates from the proband's cells (Fig. 5).

Full-length and rodless plectin transcripts are reduced in the proband's cultured fibroblasts

Using RT-PCR, the presence of mRNA that encodes full-length or rodless plectin was demonstrated in the normal human control as well as in the proband's cultured fibroblasts (Fig. 1B, 6). Judging from the PCR analysis results, the quantity of full-length and rodless plectin transcripts was markedly reduced in the proband's fibroblasts compared with those of the normal human control (Fig. 6).

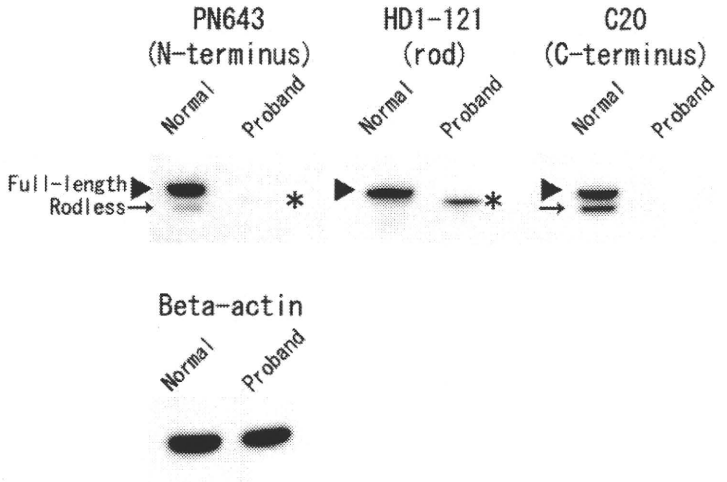

Figure 5. Immunoblot analysis of cultured fibroblasts from the normal human control and the proband. Immunoblot analysis of extracts from fibroblasts of the normal control and the proband by using PN643 against the N-terminal actin-binding domain, HD1-121 against the rod domain and C20 against the C-terminal plectin repeats. Rodless plectin (arrows), detected with PN643 and C20, migrates just below full-length plectin (arrowheads) in normal human fibroblasts. Using HD1-121, only full-length plectin is observed in the normal control. In contrast, fibroblasts of the proband contained smaller proteins than 500-kDa full-length plectin, the putatively truncated full-length plectin (asterisks), which was detected with PN643 and HD1-121. C20 did not react with lysates of the proband's fibroblasts. Equal protein loading was confirmed by reprobing with AC15 (anti-beta-actin antibody).

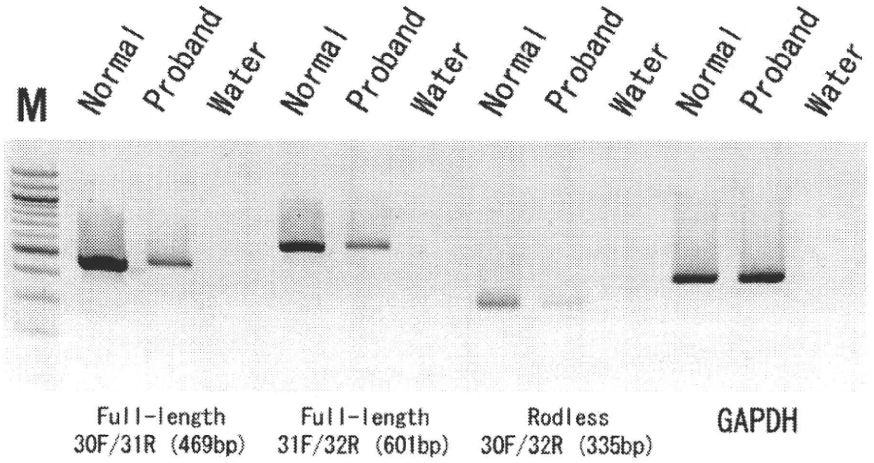

Figure 6. Semi-quantitative RT-PCR for full-length and rodless plectin transcripts. The quantity of full-length (30F/31R and 31F/32R) and rodless (30F/32R) plectin transcripts in the proband's cultured fibroblasts is reduced in comparison to those of the normal control. GAPDH mRNA expression was used as the loading control in these experiments. The negative control reaction (DNA-free water instead of cDNA) shows no PCR products. The molecular weight standard (lane M) is a 100-bp ladder.

DISCUSSION

This is the first report of EB complicated with both MD and PA. Skin detachment within basal keratinocytes was demonstrated by electron microscopy, which indicated the simplex subtype of EB. The proband's skin sample and cultured fibroblasts showed reduced and truncated plectin expression (Fig. 1D).

Both of the premature termination codon (PTC)-causing mutations detected in our case are within exon 32, the last exon of *PLEC*. Nonsense-mediated mRNA decay (NMD) is a quality-control mechanism that selectively degrades mRNAs with PTCs (Holbrook, et al., 2004). When the mRNA has a PTC more than a certain range upstream of one exon-exon junction, the transcript is down-regulated by NMD. In contrast, when PTCs are located in the last exon, NMD does not generally occur and abnormal mRNA is translated into truncated protein. However, some exceptions were described in a study in which transcripts underwent NMD despite having a PTC in the last exon (Chan, et al., 1998). Reduced amounts of full-length and rodless plectin transcripts in the proband's cells are explained by NMD, even though the PTCs of the proband are in the last exon.

One reported EBS-MD case was homozygous for a PTC-causing mutation (c.13458_13473dup) in exon 32 (Schroder, et al., 2002). c.13458_13473dup is at the downstream of the 6th plectin repeat and is predicted to cause a frameshift followed by a premature termination codon. The age of onset for MD in the patient with c.13458_13473dup was 4 years (Schroder, et al., 2002); in our case, severe muscle weakness was observed immediately after birth. This clinical difference might be explained by the length of truncated proteins identified in each patient. Compound heterozygous mutations of c.10984C>T and c.11453_11462del encode truncated plectin protein that does not include the intermediate filament (IF) binding site that was mapped to an approximately 50-amino-acid sequence between the 5th and 6th plectin repeat (Nikolic, et al., 1996; Rezniczek, et al., 2010). Therefore, the truncated plectin in our case might not have bound to IF including desmin in muscle tissues, which might account for the congenital muscle weakness. In contrast, the truncated plectin produced by c.13458_13473dup harbors the IF-binding site described above. Although the amount of plectin protein was slightly diminished, it may be that substantial amounts of truncated plectin with the residual IF-binding site delayed the development of muscular dystrophy and prevented pyloric atresia in the previous patient (Schroder, et al., 2002).

EBS-MD patients do not have muscular symptoms at birth, but muscle weakness appears later in their life. The type of *PLEC* mutations (PTC-causing mutations or in-frame insertions/deletions) influences the timing of MD onset (Chiaverini, et al., 2010). Also, it may be that, in most EBS-MD cases, the presence of residual rodless plectin resulting from PTC-causing mutations in exon 31 delays the onset of MD because of the remaining IF-binding site in rodless plectin.

It has been postulated that two pathologic elements are involved in the development of PA in EB patients: 1) the integrity of basement membrane and hemidesmosomes, and 2) the control of the normal process of fibrosis in the course of wound healing (Maman, et al., 1998). The sequence of events might be initiated by the separation of the intestinal mucosal layer as a result of disintegration of basement membrane and hemidesmosomes. Inflammatory responses cause massive fibrosis, which might lead to the obstruction of the intestinal lumina, especially in anatomically narrow passages, such as pylorus (Maman, et al., 1998). Previously described EBS-MD patients do not suffer from PA, which suggests that residual rodless plectin can prevent the development of PA. In our case, both full-length and rodless plectin proteins are quantitatively reduced and the shortened plectin might not have functioned normally, which might have lead to the PA phenotype.

It had been predicted that some cases of EBS-PA would develop MD, although no such case had been reported in the literature (Natsuga, et al., 2010). One possible explanation is that the poor systemic condition of EBS-PA and the limited observation period due to the patient's very short lifespan prevented the diagnosis of MD. Our data suggests that surgical correction of PA is insufficient to treat EBS-PA patients because they would most likely go on to develop MD even if they survive surgery. Therefore, we should look to develop more fundamental therapeutic options for those patients.

In summary, this study clearly shows that plectin mutations lead to both MD and PA phenotypes in an individual EBS patient.

ACKNOWLEDGMENTS

We thank Ms. Yuko Hayakawa and Ms. Yuki Miyamura for their technical assistance. This work was supported by Health and Labor Sciences Research grants for Research on Measures for Intractable Diseases from the Ministry of Health, Labor and Welfare of Japan (to H.S.).

Contract grant sponsor: The Ministry of Health, Labour and Welfare; Contract grant number: H20-Nanchi-Ippan-028.

REFERENCES

Chan D, Weng YM, Graham HK, Sillence DO, Bateman JF. 1998. A nonsense mutation in the carboxyl-terminal domain of type X collagen causes haploinsufficiency in schmid metaphyseal chondrodysplasia. J Clin Invest 101:1490-9.

Chiaverini C, Charlesworth A, Meneguzzi G, Lacour JP, Ortonne JP. 2010. Epidermolysis bullosa simplex with muscular dystrophy. Dermatol Clin 28:245-55, viii.

Elliott CE, Becker B, Oehler S, Castanon MJ, Hauptmann R, Wiche G. 1997. Plectin transcript diversity: identification and tissue distribution of variants with distinct first coding exons and rodless isoforms. Genomics 42:115-25.

Fine JD, Eady RA, Bauer EA, Bauer JW, Bruckner-Tuderman L, Heagerty A, Hintner H, Hovnanian A, Jonkman MF, Leigh I and others. 2008. The classification of inherited epidermolysis bullosa (EB): Report of the Third International Consensus Meeting on Diagnosis and Classification of EB. J Am Acad Dermatol 58:931-50.

Gache Y, Chavanas S, Lacour JP, Wiche G, Owaribe K, Meneguzzi G, Ortonne JP. 1996. Defective expression of plectin/HD1 in epidermolysis bullosa simplex with muscular dystrophy. J Clin Invest 97:2289-98.

Groves RW, Liu L, Dopping-Hepenstal PJ, Markus HS, Lovell PA, Ozoemena L, Lai-Cheong JE, Gawler J, Owaribe K, Hashimoto T and others. 2010. A Homozygous Nonsense Mutation within the Dystonin Gene Coding for the Coiled-Coil Domain of the Epithelial Isoform of BPAG1 Underlies a New Subtype of Autosomal Recessive Epidermolysis Bullosa Simplex. J Invest Dermatol 130:1551-7.

Holbrook JA, Neu-Yilik G, Hentze MW, Kulozik AE. 2004. Nonsense-mediated decay approaches the clinic. Nat Genet 36:801-8.

Koster J, van Wilpe S, Kuikman I, Litjens SH, Sonnenberg A. 2004. Role of binding of plectin to the integrin beta4 subunit in the assembly of hemidesmosomes. Mol Biol Cell 15:1211-23.

Laemmli UK. 1970. Cleavage of structural proteins during the assembly of the head of bacteriophage T4. Nature 227:680-5.

Maman E, Maor E, Kachko L, Carmi R. 1998. Epidermolysis bullosa, pyloric atresia, aplasia cutis congenita: histopathological delineation of an autosomal recessive disease. Am J Med Genet 78:127-33.

McLean WH, Pulkkinen L, Smith FJ, Rugg EL, Lane EB, Bullrich F, Burgeson RE, Amano S, Hudson DL, Owaribe K and others. 1996. Loss of plectin causes epidermolysis bullosa with muscular dystrophy: cDNA cloning and genomic organization. Genes Dev 10:1724-35.

Nakamura H, Sawamura D, Goto M, Nakamura H, McMillan JR, Park S, Kono S, Hasegawa S, Paku S, Nakamura T and others. 2005. Epidermolysis bullosa simplex associated with pyloric atresia is a novel clinical subtype caused by mutations in the plectin gene (PLEC1). J Mol Diagn 7:28-35.

Natsuga K, Nishie W, Akiyama M, Nakamura H, Shinkuma S, McMillan JR, Nagasaki A, Has C, Ouchi T, Ishiko A and others. 2010. Plectin expression patterns determine two distinct subtypes of epidermolysis bullosa simplex. Hum Mutat 31:308-16.

Nikolic B, Mac Nulty E, Mir B, Wiche G. 1996. Basic amino acid residue cluster within nuclear targeting sequence motif is essential for cytoplasmic plectin-vimentin network junctions. J Cell Biol 134:1455-67.

Pfendner E, Rouan F, Uitto J. 2005. Progress in epidermolysis bullosa: the phenotypic spectrum of plectin mutations. Exp Dermatol 14:241-9.

Pfendner E, Uitto J. 2005. Plectin gene mutations can cause epidermolysis bullosa with pyloric atresia. J Invest Dermatol 124:111-5.

Pulkkinen L, Smith FJ, Shimizu H, Murata S, Yaoita H, Hachisuka H, Nishikawa T, McLean WH, Uitto J. 1996. Homozygous deletion mutations in the plectin gene (PLEC1) in patients with epidermolysis bullosa simplex associated with late-onset muscular dystrophy. Hum Mol Genet 5:1539-46.

Rezniczek GA, Walko G, Wiche G. 2010. Plectin gene defects lead to various forms of epidermolysis bullosa simplex. Dermatol Clin 28:33-41.

Sawamura D, Goto M, Sakai K, Nakamura H, McMillan JR, Akiyama M, Shirado O, Oyama N, Satoh M, Kaneko F and others. 2007. Possible involvement of exon 31 alternative splicing in phenotype and severity of epidermolysis bullosa caused by mutations in PLEC1. J Invest Dermatol 127:1537-40.

Schroder R, Kunz WS, Rouan F, Pfendner E, Tolksdorf K, Kappes-Horn K, Altenschmidt-Mehring M, Knoblich R, van der Ven PF, Reimann J and others. 2002. Disorganization of the desmin cytoskeleton and mitochondrial dysfunction in plectin-related epidermolysis bullosa simplex with muscular dystrophy. J Neuropathol Exp Neurol 61:520-30.

Shimizu H, Masunaga T, Kurihara Y, Owaribe K, Wiche G, Pulkkinen L, Uitto J, Nishikawa T. 1999a. Expression of plectin and HD1 epitopes in patients with epidermolysis bullosa simplex associated with muscular dystrophy. Arch Dermatol Res 291:531-7.

Shimizu H, Takizawa Y, Pulkkinen L, Murata S, Kawai M, Hachisuka H, Udono M, Uitto J, Nishikawa T. 1999b. Epidermolysis bullosa simplex associated with muscular dystrophy: phenotype-genotype correlations and review of the literature. J Am Acad Dermatol 41:950-6.

Smith FJ, Eady RA, Leigh IM, McMillan JR, Rugg EL, Kelsell DP, Bryant SP, Spurr NK, Geddes JF, Kirtschig G and others. 1996. Plectin deficiency results in muscular dystrophy with epidermolysis bullosa. Nat Genet 13:450-7.

Takizawa Y, Shimizu H, Rouan F, Kawai M, Udono M, Pulkkinen L, Nishikawa T, Uitto J. 1999. Four novel plectin gene mutations in Japanese patients with epidermolysis bullosa with muscular dystrophy disclosed by heteroduplex scanning and protein truncation tests. J Invest Dermatol 112:109-12.

Wiche G, Becker B, Luber K, Weitzer G, Castanon MJ, Hauptmann R, Stratowa C, Stewart M. 1991. Cloning and sequencing of rat plectin indicates a 466-kD polypeptide chain with a three-domain structure based on a central alpha-helical coiled coil. J Cell Biol 114:83-99.

THE JOURNAL OF IMMUNOLOGY

Human IgG1 Monoclonal Antibody against Human Collagen 17 Noncollagenous 16A Domain Induces Blisters via Complement Activation in Experimental Bullous Pemphigoid Model

Qiang Li, Hideyuki Ujiie, Akihiko Shibaki, Gang Wang, Reine Moriuchi, Hong-jiang Qiao, Hiroshi Morioka, Satoru Shinkuma, Ken Natsuga, Heather A. Long, Wataru Nishie and Hiroshi Shimizu

J Immunol 2010;185;7746-7755; Prepublished online 12 November 2010;
doi:10.4049/jimmunol.1000667
http://www.jimmunol.org/content/185/12/7746

The Journal of Immunology is published twice each month by The American Association of Immunologists, Inc., 9650 Rockville Pike, Bethesda, MD 20814-3994.

Print ISSN: 0022-1767 Online ISSN: 1550-6606.

Human IgG1 Monoclonal Antibody against Human Collagen 17 Noncollagenous 16A Domain Induces Blisters via Complement Activation in Experimental Bullous Pemphigoid Model

Qiang Li,*,[1] Hideyuki Ujiie,*,[1] Akihiko Shibaki,* Gang Wang,* Reine Moriuchi,* Hong-jiang Qiao,* Hiroshi Morioka,† Satoru Shinkuma,* Ken Natsuga,* Heather A. Long,* Wataru Nishie,* and Hiroshi Shimizu*

Bullous pemphigoid (BP) is an autoimmune blistering disease caused by IgG autoantibodies targeting the noncollagenous 16A (NC16A) domain of human collagen 17 (hCOL17), which triggers blister formation via complement activation. Previous in vitro analysis demonstrated that IgG1 autoantibodies showed much stronger pathogenic activity than IgG4 autoantibodies; however, the exact pathogenic role of IgG1 autoantibodies has not been fully demonstrated in vivo. We constructed a recombinant IgG1 mAb against hCOL17 NC16A from BP patients. In COL17-humanized mice, this mAb effectively reproduced a BP phenotype that included subepidermal blisters, deposition of IgG1, C1q and C3, neutrophil infiltration, and mast cell degranulation. Subsequently, alanine substitutions at various C1q binding sites were separately introduced to the Fc region of the IgG1 mAb. Among these mutated mAbs, the one that was mutated at the P331 residue completely failed to activate the complement in vitro and drastically lost pathogenic activity in COL17-humanized mice. These findings indicate that P331 is a key residue required for complement activation and that IgG1-dependent complement activation is essential for blister formation in BP. This study is, to our knowledge, the first direct evidence that IgG1 Abs to hCOL17 NC16A can induce blister formation in vivo, and it raises the possibility that IgG1 mAbs with Fc modification may be used to block pathogenic epitopes in autoimmune diseases. *The Journal of Immunology*, **2010, 185: 7746–7755.**

Bullous pemphigoid (BP) is the most common autoimmune subepidermal blistering disease (1, 2). Circulating autoantibodies target human type XVII collagen (human collagen 17 [hCOL17]), also known as BP Ag 2 (BPAG2) or BP180, which is a major component in hemidesmosome-anchoring filament complexes at the epidermal basement membrane zone (BMZ) (3–9). The major pathogenic epitope of BP autoantibodies is present at the extracellular noncollagenous 16A (NC16A) domain, which has distinctive diversity among different species (10–12). Deposition of anti-hCOL17 autoantibodies at the BMZ triggers sequential inflammatory cascades, including complement activation, degranulation of dermal mast cells, infiltration of eosinophils and neutrophils, and subepidermal blister formation elicited by proteinases derived from the inflammatory cells (13–17).

In the inflammatory mechanism of BP, the IgG-dependent classical complement pathway plays an important role in autoimmune blister formation. Complement components including C1q, C3 and C4 are detected at the dermal-epidermal junction (DEJ) in the skins of patients and experimental BP model mice (17–21). BP phenotypes have been abolished by the inhibition of C1q using neutralizing Abs in experimental models (18). C1q-binding amino acid residues underlie IgG–C1q interaction, which forms an initiation complex in the classical complement pathway (22), such as in humoral immunity to pathogens. The pathogens recognized by Abs are cleared by phagocytosis, Ab-dependent cell-mediated cytotoxicity (ADCC), and complement-dependent cytotoxicity (CDC) mechanisms. Interaction of the C1q and IgG Fc region is an initial step in CDC reaction to pathogens (23). The constant 2 (C_H2) domain is the crucial region for C1q binding to the IgG Fc region (24, 25). Mapping studies of C1q-binding residues have demonstrated that the three spatially close sites (K322, P329, and P331) constitute the binding epicenter in the human IgG1 C_H2 domain. E318 and K320 have been shown to play a minor role in complement activation by site-directed mutagenesis studies in vitro. Among different species, these residues are relatively well conserved (22, 25–27). However, the precise role of these binding residues has not been determined in the activation of complement cascades in vivo.

*Department of Dermatology, Hokkaido University, Graduate School of Medicine, Sapporo; and †Faculty of Medical and Pharmaceutical Sciences, Kumamoto University, Kumamoto, Japan

[1]Q.L. and H.U. contributed equally to this work.

Received for publication February 26, 2010. Accepted for publication October 4, 2010.

This work was supported by the Program for Promotion of Fundamental Studies in Health Sciences of the National Institute of Biomedical Innovation (06-42 to H.S.) and in part by Grants-in-Aid for Scientific Research (A) (21249063 to H.S.) and (C) (20591312 to A.S.) from the Ministry of Education, Culture, Sports, Science, and Technology of Japan.

Address correspondence and reprint requests to Dr. Akihiko Shibaki and Dr. Hiroshi Shimizu, Department of Dermatology, Hokkaido University Graduate School of Medicine, North 15 West 7, Kita-ku, Sapporo, 060-8638, Japan. E-mail addresses: ashibaki@med.hokudai.ac.jp and shimizu@med.hokudai.ac.jp

The online version of this article contains supplemental material.

Abbreviations used in this paper: ADCC, Ab-dependent cell-mediated cytotoxicity; BMZ, basement membrane zone; BP, bullous pemphigoid; C1q, complement 1q; CDC, complement-dependent cytotoxicity; C_H2, constant 2; COL17, type XVII collagen; DB, dilution buffer; DEJ, dermal-epidermal junction; DIF, direct immunofluorescence; Flu, fluorescence; HSC, human serum complement; IIF, indirect immunofluorescence; NC16A, noncollagenous 16A; NHEK, normal human epidermal keratinocyte; PI, propidium iodide; rh, recombinant human; Sf-9, *Spodoptera frugiperda*-9; VH, V region H chain; VL, V region L chain.

www.jimmunol.org/cgi/doi/10.4049/jimmunol.1000667

IgG1 is thought to be the predominant subclass of anti-hCOL17 IgG autoantibodies in sera from BP patients. Clinical studies have shown a preferential detection of hCOL17-specific IgG1 and IgG4 autoantibodies in BP sera, with IgG2 and IgG3 being detected in a minority of patients (5, 7, 28). Eighty-five percent and 46% of BP sera contained IgG1 and IgG4 Abs against hCOL17, respectively (6). The presence of IgG1 autoantibodies has been associated with active BP phenotypes (5, 6), and the autoantibody level has been correlated with the area of skin blistering (29). These clinical findings indicate that IgG1 might be the main pathogenic subclass in BP. However, to our knowledge, there has been no direct in vivo evidence to demonstrate the pathogenic role of the anti-hCOL17 IgG1 autoantibody until now.

To confirm whether BP IgG1 autoantibodies can induce the BP phenotype in vivo and to analyze the importance of various C1q-binding residues in the IgG1 Fc C_H2 domain in BP, we cloned and constructed a recombinant human (rh)IgG1 mAb against hCOL17 NC16A. By site-directed mutagenesis in the C_H2 domain of the IgG1 mAb Fc region, alanine substitutions were introduced at various residue sites that were previously verified as C1q binding sites in vitro. The blister formation triggered by the non-mutated IgG1 mAb was assessed in vivo using our COL17-humanized ($COL17^{m-/-,\ h+}$) mouse model, which expresses hCOL17 but not mouse COL17 at the BMZ (17). In contrast, the IgG1 mAbs that were mutated at the P331 and/or P329 residue(s) failed to elicit blister formation. Our findings indicate that IgG1 Abs, as the predominant IgG subclass, can induce subepidermal blister formation via IgG Fc–C1q interaction in BP.

Materials and Methods

Establishment of the EBV-transformed B cell clones

PBMCs were prepared from seven active nontreated BP patients by density gradient using Ficoll-Paque PLUS (GE Healthcare, Uppsala, Sweden). The diagnosis of BP was made by the typical clinical and histological manifestations as well as by laboratory data including anti-hCOL17 ELISA and indirect immunofluorescence (IIF). The clinical and immunological characteristics of the BP patients are summarized in Supplemental Table I. B cells were isolated by using microbeads conjugated to anti-human CD19 mAb (Miltenyi Biotec, Bergisch Gladbach, Germany), followed by seeding at 15 cells/well in 96 U-bottom microplates (BD Biosciences, San Jose, CA) in complete RPMI 1640 medium containing 2.5 μg/ml ODN2006 (InvivoGen, San Diego, CA) and incubation for 2 wk with irradiated cord mononuclear cells as the feeder layer cells (50,000/well) in the presence of EBV (30% supernatant of B95.8 cells). The culture supernatants were tested for the presence of anti-hCOL17 NC16A Abs by ELISA coated with rhCOL17 NC16A peptide as reported previously (17). The index values of ELISA were defined by the following formula: index = (OD of tested supernatant − OD of negative control)/(OD of positive control − OD of negative control) × 100 (30–32). As a positive control, we used a standard BP serum supplied with the hCOL17 NC16A-ELISA kit (MESACUP BP180 test; Medical and Biological Laboratories, Nagoya, Japan) as reported previously (17, 33). Adjustment of the values relative to the positive control allows comparison of results from different plates, even if performed under different conditions. Positive wells were cloned by limiting dilution in the presence of ODN2006 and irradiated cord mononuclear cells.

Construction of IgG1 expression vector

L chain (κ and λ) and Fd (V region + constant domain 1) fragments were amplified by RT-PCR from monoclonal B cell clones using general primers for the Ab library (Table I), cloned into pCR2.1 vectors (Invitrogen, Carlsbad, CA), and sequenced by ABI 3100 genetic analyzer (Applied Biosystems, Foster, CA). After introducing one cutting site by the restriction endonucleases EcoRV at the 3′ end, the L chain was inserted into the human IgG1 expression vector pAc-κ-Fc or pAc-λ-Fc (Progen, Heidelberg, Germany) at the SacI and EcoRV cutting sites (Supplemental Fig. 1). Then the Fd sequence was inserted into the vector at the XhoI and SpeI cutting sites. The constructed baculovirus vector containing Fd and $V_{\kappa \text{ or } \lambda}$ genes was transfected to *Spodoptera frugiperda*-9 (Sf-9) insect cells using the BaculoGold Transfection Kit (BD Biosciences). Recombinant baculovirus was harvested from the supernatant of Sf-9 cell culture medium TNM-FH (Grace's insect medium, 10% FBS, and penicillin-streptomycin) (Invitrogen) at 4–5 d after the transfection. Secreted rhIgG1 Abs were detected in the supernatant using an hCOL17 NC16A-ELISA kit (MBL, Nagoya, Japan). The whole procedure followed the manufacturers' recommendations.

Production and purification of the rhIgG1 mAb

The recombinant virus inocula, via three rounds of plaque purification, infected Sf-9 cells at a multiplicity of infection of 0.5–10. The cells were grown in SF-900 II SFM (Life Technologies, Carlsbad, CA) serum-free suspension culture using a spinner 1-L flask with a vertical impeller (Corning, Lowell, MA) at 27°C. One week later, supernatant was harvested and clarified by centrifugation and filtered through 0.45 μM filters (Millipore, Bedford, MA). Purification was performed on HiTrap Protein G column (GE Healthcare). The eluted IgG in 1 M glycine-HCl (pH 2.7) was dialyzed in PBS for at least 48 h and then quantified by spectrophotometer (Pharmacia Biotech, Uppsala, Sweden) at 280 nm.

Generation of the mutated IgG1 mAbs

Alanine substitutions were incorporated into the human IgG1 pAc-λ-Fc vector by site-directed mutagenesis using a Quick Change Mutagenesis Kit (Stratagene, La Jolla, CA), according to the manufacturer's instructions. We constructed seven mutants: five single-site ones and two multisite ones. The mutagenic oligonucleotide primers containing target sites are listed in Table I. Primers were purified by PAGE to prevent the primers from experiencing a significant decrease in mutation efficiency. Sequences were verified by ABI 3100 genetic analyzer (Applied Biosystems). The different constructs were expressed in the Sf-9 cells described above. The IgG was directly purified from the filtered serum-free supernatant using 5 ml HiTrap Protein G column (GE Healthcare).

Establishment of hCOL17-293 cells

To establish the hCOL17-293 cell line, FlpIn 293 cells (Invitrogen) were first cotransfected with the constructed plasmid pcDNA5/FRT (Invitrogen) that had been inserted with the hCOL17 gene (a gift from Dr. K. B. Yancey, University of Texas Southwestern Medical Center, Dallas, TX) and pOG44 (Invitrogen) and were then cultured in selective medium (DMEM, 100 μg/ml hygromycin B [Invitrogen], and 10% FBS). Second, the expression levels of hCOL17 were detected by Western blot analysis using BP serum Abs (1:20) as the first Ab. Eventually, the positive clones were maintained in DMEM containing 50 μg/ml hygromycin B and 10% FBS. The procedures were handled according the manufacturers' recommendations.

Epitope mapping of the IgG1 mAb

We synthesized the N terminus half (hNC16A 1–3, aa 490–534) of the hCOL17 NC16A domain as a GST-fusion protein using the expression vector pGEX2-T (Amersham Biosciences, Uppsala, Sweden) and bacteria B12 (Amersham Biosciences), as reported previously (17, 34). Other peptides including hNC16A 1 (aa 490–506), hNC16A 2 (aa 506–520), hNC16A 2.5 (aa 514–532), and hNC16A 3 (aa 520–534) were expressed in the same way and then purified with a GSTrap FF affinity column (GE Healthcare). The purified IgG1 mAb 3.B6 (0.25 μg/ml) was incubated with the 0.5 μg/lane GST-fusion proteins that were transferred to a 0.2-μm nitrocellulose membrane (Bio-Rad, Richmond, CA) for storage at 4°C overnight. Immunoblots were probed with anti-human IgG polyclonal Abs conjugated with HRP (1:1000; DakoCytomation, Glostrup, Denmark). BP serum from patient 3 (1:30) was acted as the positive control.

Competitive-inhibition assay

Competitive-inhibition ELISA was performed in triplicate as described previously (35). Inhibitor solutions (five subpeptides of the hNC16A, full-length hNC16A, and GST protein) were double serially diluted in 0.5% BSA and mixed with equal volumes of the IgG1 mAb 3.B6 (2.5 μg/ml), then incubated at 37°C for 1 h. One hundred microliters of the mixtures was added to the wells coated with hCOL17 NC16A. The remainder of the assay was performed according to standard procedures. OD was measured at 450 nm.

C1q-binding assay

The C1q-binding activity of the mutated IgG1 mAbs was determined by C1q ELISA-binding assay. The mAbs with double serial dilution (starting concentration: 20 μg/ml) in 0.05 M sodium carbonate buffer (pH 9) were coated in a 96-well plate (Nalge Nunc International, Rochester, NY) and left overnight at 4°C. The plates were washed three times with PBS containing 0.05% Tween 20 and blocked for 1 h at room temperature with

ELISA diluent buffer (BD Biosciences), then incubated for 2 h with 100 μl 4 μg/ml human complement component C1q (Sigma-Aldrich, St. Louis, MO) in ELISA diluent buffer. Then, 100 μl of a 1:400 dilution of sheep polyclonal to C1q (HRP) (Abcam, Tokyo, Japan) was added after washing, and incubation was done for 1 h. Plates were washed five times and displayed in tetramethylbenzidine-soluble reagent (ScyTek, Logan, UT) and then stopped by the addition of 50 μl 20% H_2SO_4 (Wako, Osaka, Japan). The OD was determined at 450 nm. To correct for background, the OD at 450 nm was subtracted from the OD at 620 nm. Binding activity was calculated by the following formula: index value = $(OD_{test} - OD_{blank})/(OD_{St.} - OD_{blank})$, where St. is standard human IgG1 (BD Biosciences) and blank is the diluent buffer.

CDC assay

Serum complements from human (Quidel, San Diego, CA) and mouse (Innovative, Novi, MI) were used for cytotoxicity assay. The mAbs (20–0.04 μg/ml) were diluted with dilution buffer (DB) (DMEM [Life Technologies] [pH 7.2], 2 mM glutamine, 0.1% BSA, and 50 μg/ml hygromycin). The hCOL17-293 cells were washed in DB and resuspended at a density of 10^6 cells/ml. In a typical assay, 50 μl of the mAbs, 50 μl diluted complement, and 50 μl cell suspension were added to flat-bottom tissue culture 96-well plates. The mixture was incubated for 2 h at 37°C in 5% CO_2 incubator to facilitate cell lysis. Then, 50 μl Alamar Blue (Invitrogen) diluted in the DB was added to each well and incubated overnight at 37°C in 5% CO_2 incubator. Fluorescence (Flu) value was monitored at 530-nm excitation wavelength and 630-nm emission wavelength using a 96-well Fluorometer (Berthold, Tokyo, Japan). Reduced Flu units exhibit proportionally to the number of viable cells. The activity of the various mutants was examined by plotting the percent CDC activity against the log of working concentration of the mAb. The Flu value of triplicates was used to calculate the percent cytotoxicity: percent CDC activity = $100 \times (1 - [Flu_{no\ complement} - Flu_{test}]/[Flu_{no\ complement} - Flu_{total\ lysis}])$, where $Flu_{total\ lysis}$ reading from positive control well was incubated for an additional 15 min with lysis solution (Roche, Mannheim, Germany).

ADCC assay

The normal PBMCs were fractionated by Ficoll-Paque PLUS gradient and resuspended in assay reaction buffer (RPMI 1640, 10 mM HEPES, 1% FBS, and 100 μg/ml gentamycin). The hCOL17-293 cells were washed and resuspended in the assay reaction buffer. Double-serial-diluted mAb in a 50-μl assay reaction buffer was incubated with 50 μl target cells (hCOL17-293 cells) (10,000 cells/well) for 30 min at 37°C. Then 50 μl effector cells (normal PBMCs) in a cell suspension (100,000 cells/well) was dispensed into the wells, and incubation was continued for 4 h at 37°C. The activity of lactate dehydrogenase was determined by using the Cytotoxicity Detection PLUS (lactate dehydrogenase) Kit (Roche), according to the manufacturer's instructions. The absorbance (450 nm) of triplicates was used to calculate the percent cytotoxicity: percent cytotoxicity = $100 - 100 \times (OD_{test} - OD_{background})/(OD_{total\ lysis} - OD_{background})$, where $OD_{total\ lysis}$ reading from the positive-control well was incubated for an additional 15 min by lysis solution (Roche).

Passive-transfer models

The Abs including the nonmutated, mutated, BP and healthy serum IgGs were individually injected into 1-d neonatal COL17-humanized ($COL17^{m-/-,\ h+}$) mice at a dose of 25–200 μg/g body weight as described previously (17). At 48 h after i.p. injection of the IgG Abs, skin blister formation was assessed by gentle skin friction. Back skin was used for histological examination (Genetic-Lab, Sapporo, Japan) and direct immunofluorescence (DIF) test using FITC-conjugated polyclonal Ab to human IgG (1:100) (DakoCytomation), murine C1q (1:40) (MBL), and murine C3 (1:200) (Abcam).

Immunofluorescence

Immunofluorescence analysis using the nonmutated or mutated IgG1 mAbs was performed on adult $COL17^{m-/-,\ h+}$ mouse tail, neonatal $COL17^{m-/-,\ h+}$ mouse skin, and normal human skin as described previously (17). Flu labeling was performed with FITC-conjugated secondary Abs (1:100) (DakoCytomation), followed by 10 μg/ml propidium iodide (PI) (Sigma-Aldrich) to counterstain the nuclei. The stained samples were observed and photographed under a confocal laser scanning microscope (Olympus Fluoview FV1000; Olympus, Tokyo, Japan).

Ethical considerations

This study was approved by the Institutional Review Board of Hokkaido University (Sapporo, Japan) and fully informed consent from all patients was obtained for use of human material. All animal operations were approved by and performed in accordance with the Institutional Lab Animal Care and Use Committee of Hokkaido University.

Statistics

Data values were shown as means and/or percentages. We determined statistical significance using Student t test or Pearson χ^2 test. One-way or two-way ANOVA test was used for comparing the C1q-binding, CDC, and ADCC activities of the nonmutated and mutated mAbs. A p value <0.05 or 0.01 was considered statistically significant. Analysis was carried out using the statistical software SPSS 10.0 (SPSS, Chicago, IL).

Results

Establishment of immortalized B cell clones derived from BP patients

By means of EBV transformation and limiting dilution (36), three immortalized B cell clones (3.B6, 1.F5, and 7.H8) were established from PBMCs of the seven active BP patients (3.B6 from patient 3, 1.F5 from patient 1, and 7.H8 from patient 7). These three clones stably grew and secreted the IgG mAbs against hCOL17 NC16A. ELISA analysis showed that all the supernatants from the three clones (3.B6, 1.F5, and 7.H8) recognized the rhCOL17 NC16A protein (respective index values [mean ± SD]: 82.99 ± 4.32, 40.18 ± 2.53, and 30.79 ± 1.61). The IgG subclasses of the three clones are IgG1, IgG1, and IgG4, respectively, as determined by gene sequencing. IIF analysis using normal human skin revealed that the supernatants of both 3.B6 and 1.F5 showed linear IgG deposition at the BMZ (Fig. 1*A*, 1*B*). In contrast, the supernatant of clone 7.H8 failed to recognize the BMZ (Fig. 1*C*). We then generated rhIgG1 mAbs containing the Fab regions of these three immortalized B cell clones.

Generation of rhIgG1 mAbs against hCOL17 NC16A

To construct rhIgG1 mAbs, we amplified and cloned the cDNA that encodes IgG L and H chain variable domains ($V_{\kappa\ or\ \lambda}$ and Fd) from the immortalized B cell clones by RT-PCR using Ab library general primers (Table I). The 700-bp L/H chain variable genes (VL/VH) of clones 3.B6, 1.F5, and 7.H8 were cloned and ampli-

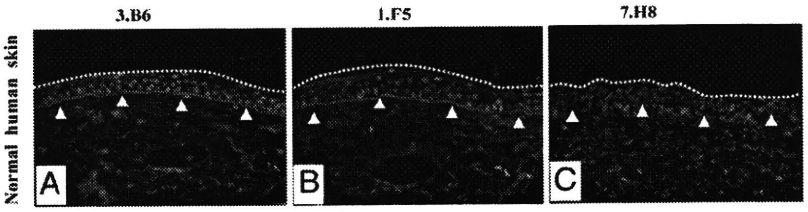

FIGURE 1. Characterization of immortalized B cell clones. IIF analysis was used for detecting the immunoreactivity of the IgG supernatant collected in the first week with normal human skin. Rabbit polyclonal Abs against the H and L chains of human IgG (DakoCytomation) conjugated with FITC were used as secondary Abs (1:100). IgG in the diluted supernatant (1:1) from 2 clones 3.B6 (*A*) and 1.F5 (*B*) deposits linearly (green, FITC) at the DEJ (white arrowheads) (skin surface, white dotted line). Negative staining is observed from clone 7.H8 (*C*). Cell nuclei (red) were counterstained with PI. Original magnification ×200 (*A–C*).

Table I. *General RT-PCR primers for cloning variable genes (V) and the mutagenic primers for substituting alanines at C1q binding sites*

Primers for κ-chain	
HK5	GAMATYGAGCTCACSCAGTCTCCA
HK3	GCGCCGTCTAGAACTAACACTCTCCCCTGTTGAAGCTCTTTGTGACGGGCAAG
Primers for λ-chain	
HL5	CASTYTGAGCTCACKCARCCGCCCTC
HL3	GAGGGATCTAGAATTATGAACATTCTGTAGG
Primers for Fd	
$H_{1,3}$	CAGGTGCAGCTGGTGSAGTCTGG
H_2	CAGGTCAACTTGAAGGAGTCTGG
H_4	CAGGTGCAGCTGCAGGAGTCGGG
V_H5	CAGGTGCAGCTCGAGSAGTCTGG
HG3	GCATGTACTAGTTTTGTCACAAGA
Single-site mutagenic primers	
E318→A	TGGCTGAATGGCAAGGCGTACAAGTGCAAGGTC
K320→A	GCTGAATGGCAAGGAGTACGCGTGCAAGGTCTCCAACAAA
K322→A	GCAAGGAGTACAAGTGCGCGGTCTCCAACAAAGCCC
P329→A	CAACAAAGCCCTCGCAGCCCCCATCGA
P331→A	AGCCCTCCCAGCCGCCATCGAGAAAACC
Multisite mutagenic primers	
E318A K320A K322A	GACTGGCTGAATGGCAAGGCGTACGCGTGCGCGGTCTCCAACAAAGCCCTC
P329A P331A	CAACAAAGCCCTCGCAGCCGCCATCGAGAAAAC

General primers for V_L and Fd chains (M = A, C; Y = C, T; S = G, C; K = G, T; R = A, G). Mutagenic primers at C1q binding sites (only showing the sense primer; the underlined codons are substituted into alanines).

fied by the V_λ/$VH_{1,3}$ V_κ/VH_2, and V_κ/$VH_{1,3}$ subfamily primers, respectively (Table II). Details of the variable gene sequence from the clones are summarized in Supplemental Table II.

Both the VL and VH genes were successively cloned into XhoI/SpeI and SacI/EcoRV sites of the pAc-κ-Fc or pAc-λ-Fc baculovirus IgG1 expression vectors (Supplemental Fig. 1) (37). Recombinant baculovirus was produced by transfecting the recombinant vectors that contained VL/VH genes into Sf-9 insect cells. Postinfection with the purified recombinant baculovirus, the Sf-9 cells secreted rhIgG1 mAbs in the culture supernatant. ELISA analysis showed that the rIgG1 mAb from the clone 3.B6 recognized hCOL17 NC16A (index value [mean ± SD]: 161 ± 5.37) but not the unrelated control protein, human type VII collagen (index value: 2.2 ± 0.04). The human COL17 NC16A ELISA index values of mAbs derived from clones 1.F5 and 7.H8 were 4.23 ± 0.02 and 1.74 ± 0.01, respectively, which are significantly lower than that of clone 3.B6 ($p < 0.01$). This result indicates that the reactivity and/or affinity of IgG Abs secreted from insect cells was altered from those produced by human B cells, possibly as a result of differences in three-dimensional structure, to glycosylation or to other factors, even if the Abs had the same gene sequences as the variable regions (38, 39). For example, N-deglycosylation was even observed to affect the m.w. of the H or L chains of Ch-K20-sf9 (37). IIF analysis demonstrated that the rIgG1 mAb 3.B6 reacted with the BMZ of normal human (Fig. 2*A*) and COL17-humanized ($COL17^{m-/-,\ h+}$) mouse skin (Fig. 2*B*) but not with the wild-type mouse skin (Fig. 2*C*).

The amount of the mAb 3.B6 in the supernatant of the infected Sf-9 cells ranged from 5 to16 μg/ml, values that were determined by sandwich ELISA using sheep anti-human Fab Abs. Kinetic analysis using the Biacore system demonstrated that the mAb 3.B6 had high affinity for $K_D = 5.3 \times 10^{-9}$ M ($K_d = 1.9 \times 10^{-4}$ 1/s; $K_a = 3.6 \times 10^4$ 1/Ms; $K_D = K_d/K_a$). The purified mAb 3.B6 stained the cell surface of the normal human epidermal keratinocytes (Fig. 2*D*) and 293 cells that had been transfected with the hCOL17 gene (Fig. 2*E*), suggesting that this mAb recognizes the extracellular domain of hCOL17.

Table II. *Usage of Ab general primers for cloning variable genes from the B-cell clones*

B Cell Clone	L Chain	VL Subfamily	H Chain	VH Subfamily
3.B6	V_λ	VL1-JL3b	$VH_{1,3}$	VH1-D4-JH6
1.F5	V_κ	VK1-JK3	VH_2	VH2-D6-JH4
7.H8	V_κ	VK1-JK2	$VH_{1,3}$	VH3-D5-JH6

Epitope mapping by Western blot analysis using the rNC16A subpeptides revealed that the mAb 3.B6 specifically reacted with the full-length hNC16A, hNC16A 1–3, hNC16A 2, and hNC16A 2.5 (Fig. 3*A*, 3*B*). Binding inhibition assays demonstrated that two peptides (hNC16A 2 and hNC16A 2.5) sharing seven amino acids inhibited the binding of mAb 3.B6 to the hNC16A in a dose-dependent manner (Fig. 3*C*). Thus, the mAb 3.B6 specifically recognized an epitope present at subregion 2 of the hNC16A domain, which was also recognized by the serum derived from the same donor (patient 3) (Fig. 3*B*).

Generation of rhIgG1 mAbs with mutations at C1q binding sites and characterization of C1q-binding activity

After the binding activity of the IgG1 mAb 3.B6 was verified, site-directed mutagenesis was introduced at the C1q binding sites in the C_H2 domain of the rhIgG1 Fc region. Five independent residues (E318, K320, K322, P329, and P331) were substituted with alanine by single-site or multisite (E318 K320 K322 or P329 P331) mutation in the C_H2 domain. Both IIF and Western blot analysis demonstrated that all the mutated mAbs reacted to the hCOL17 NC16A as specifically as the nonmutated mAb did (data not shown). Kinetic analysis also demonstrated that the mutated mAbs had similar affinity with the nonmutated IgG1 mAb 3.B6 (data not shown).

In contrast, all the mutated mAbs demonstrated significantly reduced binding ability to C1q compared with that of the nonmutated mAb ($p < 0.01$) (Fig. 4). The binding abilities of E318A and K320A were slightly lower than that of the nonmutated mAb. No significant difference was observed between the two mutated mAbs ($p > 0.05$). The K322A, E318A K320A K322A, and P329A mAbs showed half the binding ability of the nonmutated mAb. There were no significant differences among these three mAbs ($p > 0.05$). Alanine substitution at position P331 or P329 P331 seemed to demonstrate the lowest C1q-binding capacity of

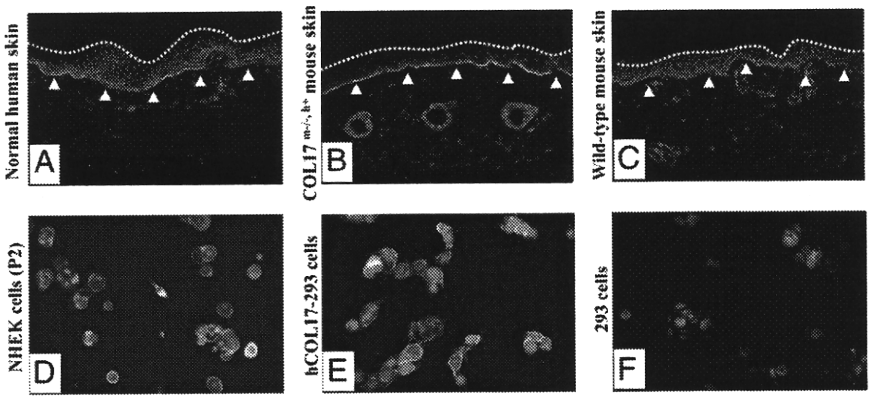

FIGURE 2. Characterization of rhIgG1 mAb 3.B6. Analysis on the specificity of mAb by IIF assay shows that the mAb (green, FITC) deposits linearly at the DEJ (white arrowheads) (skin surface, white dotted line) of normal human (*A*) and COL17-humanized ($COL17^{m-/-,h+}$) mouse skin (*B*), but does not deposit in the wild-type mouse skin (*C*). At the cellular level, the mAb binds to the plasma membrane (green) of second-passage normal human epidermal keratinocytes (NHEKs, P2) (*D*) and hCOL17-293 cells (*E*), but does not bind to 293 cells (negative control) (*F*). Red shows nuclear staining by PI. Original magnification ×100 (*A–C*); ×400 (*E*, *F*).

any of the mutated mAbs. These data indicate that P331 is the most important residue for IgG1 Fc–C1q interaction, followed by the P329, K322, K320, and E318 binding sites in the C1q-binding motif of the Fc C_H2 domain.

In vitro characterization of the CDC and ADCC activities of the mutated IgG1 mAbs

To test the ability of the mutated IgG1 mAbs to activate complement cascade in vitro, CDC assay was carried out using the hCOL17-293 cells as target cells. At 1:20 dilution of human serum complement (HSC), the nonmutated mAb showed the highest CDC activity (Fig. 5*A*). The CDC activity of the two mutated mAbs (E318A and K320A) was nearly half that of the nonmutated mAb, followed in decreasing order by K322A, E318A K320A K322A, and P329A. Their CDC activity was about one-third that of the nonmutated mAb. The mutants P331A and P329A P331A showed very low CDC activity. When the HSC concentration was increased, the percentage of CDC activity increased in the mutants E318A, K320A, K322A, P329A, and E318A K320A K322A (Fig. 5*B*, 5*C*). In contrast, no obvious change was observed in the CDC activity for P331A or P329A P331A, even at the highest HSC concentration (Fig. 5*C*). Similar results were shown when mouse serum complement was used instead of HSC (Fig. 5*D–F*). Taken together, these results indicate that all five residues of the IgG1 C_H2 domain play at least moderate roles and that P331 is the most important residue for activating complements in vitro.

To further investigate whether these mutations affect the Fc-FcγR–mediated ADCC activity of the IgG1 mAbs, we analyzed the mutated mAbs for ADCC activity using the hCOL17-293 cells as target cells and normal PBMCs as effector cells. The mutated mAbs (E318A, K320A, K322A, and E318A K320A K322A) exhibited ADCC activity similar to that of the nonmutated mAb

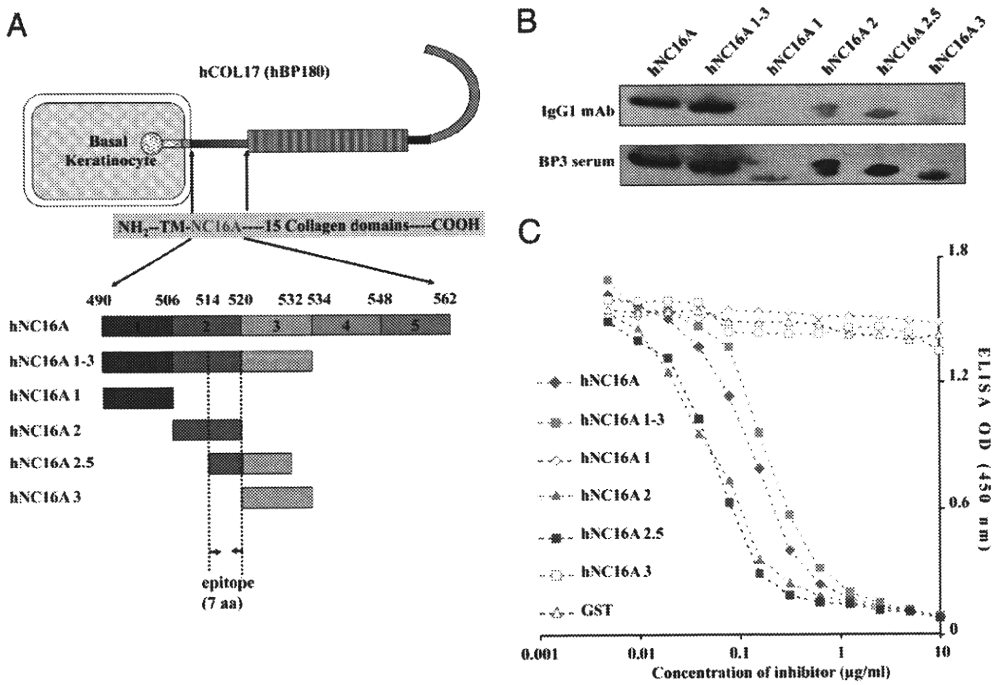

FIGURE 3. Epitope mapping of the IgG1 mAb 3.B6. A schematic map of hCOL17 (hBP180) showing the location of the hNC16A domain and the subpeptides synthesized for epitope mapping studies (*A*). Western blot analysis reveals that the IgG1 mAb recognizes the following subpeptides: hNC16A full-length (aa 490–562), hNC16A 1–3 (aa 490–534), hNC16A 2 (aa 506–520), and hNC16A 2.5 (aa 514–532) (*B*). Two subpeptides (hNC16A 1 and 3) other than the abovementioned four are also recognized by the BP serum from the same donor (patient 3). In ELISA inhibition assay (*C*), the IgG1 mAb 3.B6 (2.5 μg/ml) was incubated with the five subpeptides as inhibitor (10–0.005 μg/ml), with GST protein acting as negative control and hNC16A acting as positive control. The index value of the binding of mAb 3.B6 to the full-length hNC16A was detected by ELISA at OD 450 nm. The three subpeptides (hNC16A 1–3, hNC16A 2, and hNC16A 2.5) almost completely inhibited the binding activity of the IgG1 mAb 3.B6 in a dose-dependent manner. No significant difference in mean inhibitory activity was observed among the three subpeptides ($p > 0.05$ by two-way ANOVA test).

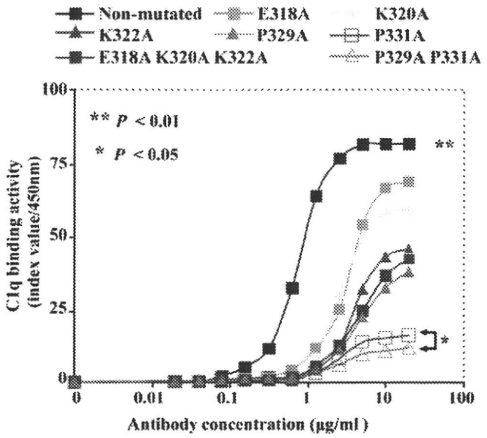

FIGURE 4. C1q-binding activity of the mutated IgG1 mAbs. The ELISA Index value of C1q binding increases gradually with increases in the IgG1 Ab. Maximal binding activity in descending order is nonmutated, then E318A, K320A, K322A, E318A K320A K322A, P329A, P331A and P329A P331A mutated mAbs. Mean index value is higher for the nonmutated mAb than for any other mutated mAbs ($p < 0.01$ by two-way ANOVA test). There is no significant difference in mean index value for E318A versus K320A or for K322 versus E318A K320A K322A or P329A ($p > 0.05$ by one-way ANOVA test). Significant difference is seen between P331A and P329A P331A ($p < 0.05$ by one-way ANOVA test).

(Fig. 6). In contrast, the substitutions at P329 or P329 P331 almost completely eliminated the ADCC activity of the mAbs ($p < 0.01$). Alanine substitution at the P331 site partially decreased the ADCC activity ($p < 0.05$). Altogether, these results suggest that P329 is a critical residue for IgG1–FcγR interaction in vitro.

In vivo functional characterization of the nonmutated and mutated IgG1 mAbs using a COL17-humanized (COL17$^{m-/-,\ h+}$) BP mouse model

To investigate the pathogenic activity of the nonmutated and mutated IgG1 mAbs in vivo, we performed a passive-transfer experiment using neonatal COL17-humanized (*COL17$^{m-/-,\ h+}$*) mice that we had established recently (17). Forty-eight hours after i.p. injection of the nonmutated IgG1 mAb (200 μg/g body weight), eight of nine neonatal mice became erythematous and showed BP-like skin blistering by gentle skin friction (Fig. 7*A*, Table III). Histopathologic examination of the recipient mouse skin confirmed the formation of subepidermal blistering (Fig. 7*B*), infiltration of lymphocytes and neutrophils (Fig. 7*C*), and degranulation of mast cells (Fig. 7*D*). DIF examination revealed the linear deposition of human IgG (Fig. 8*A*) at the BMZ, as well as of mouse C1q (Fig. 8*B*) and C3 (Fig. 8*C*). Administration of the lower dose of the nonmutated IgG1 mAb (100, 50, or 25 μg/g body weight) resulted in a lower frequency of phenotypic changes (five of seven, four of seven, or zero of five mice, respectively) (Table III). ELISA analysis of the sera of recipient mice revealed that the mean index value of the circulating anti-hCOL17 NC16A IgG1 mAbs declined from 55.39 (200 μg/g body weight) to 43.74, 36.91, and 26.53 (100, 50, and 25 μg/g body weight, respectively). Similar results were observed in positive control models with BP patients' IgG autoantibodies (data not shown) in which the BP phenotype was induced as described previously (17).

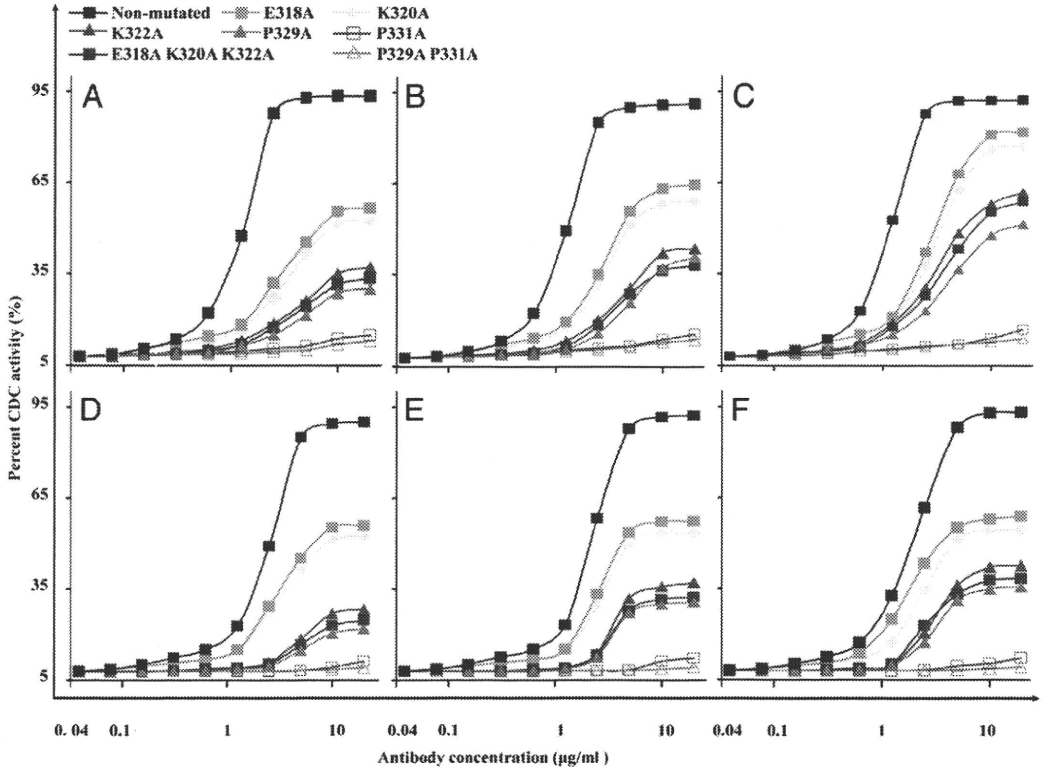

FIGURE 5. Characterization of in vitro CDC activity for the mutated IgG1 mAbs. The nonmutated mAb has the highest percent CDC activity ($p < 0.01$ by one-way ANOVA test) at HSC dilution of 1:20 (*A*), 1:10 (*B*), and 1:5 (*C*), as well as at murine serum complement dilutions of 1:20 (*D*), 1:10 (*E*), and 1:5 (*F*). E318A and K320A have significantly higher CDC activity than K322A, P329A, and E318A K320A K322A ($p < 0.01$ by two-way ANOVA test). No significant difference in the mean percent activity is seen for E318A versus K320A or for K322A versus P329A or versus E318A K320A K322A ($p > 0.05$ by one-way ANOVA test). P331A and P329A P331A show no CDC activity. Significant differences are seen for the two mAbs versus the other mAbs ($p < 0.01$ by two-way ANOVA test).

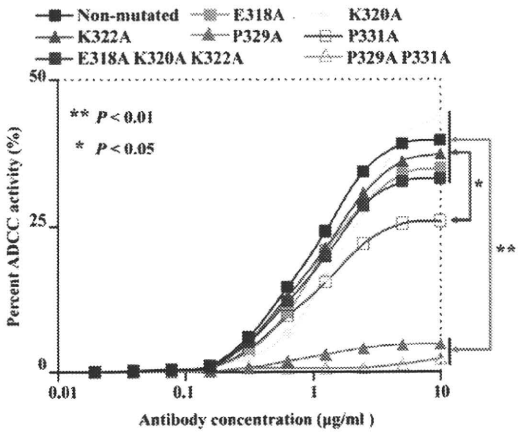

FIGURE 6. Characterization of in vitro ADCC activity for the mutated IgG1 mAbs. In IgG1 mAb-dependent cell-mediated cytotoxicity (ADCC) assay, normal human PBMCs were applied as the effector cells, and hCOL17-293 cells were the target cells. No significant differences in ADCC percent activity are shown for the E318A, K320A, K322A, and E318A K320A K322A versus the nonmutated mAbs ($p > 0.01$ by one-way ANOVA test). ADCC activity is higher for these four mAbs than for P331A ($p < 0.05$ by two-way ANOVA test). The mAbs P329A and P329A P331A show almost no ADCC activity, and significance differences are observed versus the others and nonmutated mAb ($p < 0.01$ by two-way ANOVA test).

In contrast, IgG1 mAbs with the double-site mutation (P329A P331A) completely failed to induce the BP phenotype (zero of eight mice) at the highest dose (200 μg/g body weight), whereas IgG1 mAbs with single-site mutation (P329A or P331A) showed significantly reduced pathogenic capability (one of seven or one of eight mice, respectively) compared with nonmutated IgG1 mAb ($p < 0.01$) (Figs. 7*I–L*, 8*G–I*, Table III). The other three IgG1 mAbs with a single-site mutation (E318A, K320A, or K322A) that showed high or moderate complement activity in vitro elicited skin detachment in the majority of mice at the highest dose (200 μg/g body weight) and demonstrated pathogenic activities in a dose-dependent manner as was true for the non-mutated IgG1 mAb (Figs. 7*E–H*, 8*D–F*). There were no significant differences in positive ratio of skin detachment between these three mAbs and the nonmutated mAb ($p > 0.05$) (Table III). No significant differences were observed in the hCOL17 NC16A-ELISA index values (mean values) of the circulating human IgG Abs in the recipient sera among the mutated or nonmutated IgG1 mAb models at the dose of 200 μg/g body weight ($p > 0.01$).

Discussion

This study provides, to our knowledge, the first direct evidence that human IgG1 Abs against hCOL17 NC16A can induce subepidermal blisters in vivo. BP phenotypic features, including dermal-epidermal separation, deposition of IgG1 Abs C1q and C3, recruitment of neutrophils, and degranulation of mast cells, were successfully reproduced in COL17-humanized ($COL17^{m-/-,\ h+}$) mice by the administration of human IgG1 mAbs against human COL17 NC16A, although the components of the immune system, such as complements and inflammatory cells, are still of murine origin in this experimental model.

It is well known that various IgG subclasses have distinct functional properties. IgG1 and IgG3 are the most effective complement activators, whereas IgG4 is not capable of fixing complements (40). Previous clinical studies demonstrated that IgG1 and IgG4 autoantibodies are major IgG subclasses of BP patient autoantibodies and that IgG2 and IgG3 are minor subclasses of BP patient autoantibodies (5, 7, 28). In vitro analysis using cryosections of human skin and leukocytes from healthy volunteers demonstrated that IgG1 autoantibodies purified from BP sera showed much stronger pathogenic activity than that of IgG4 autoantibodies (41). However, there has been no direct evidence of pathogenic activity of IgG1 autoantibodies in a BP model in vivo. Our group and others have successively reproduced BP phenotypes in COL17-humanized mice by administering IgG autoantibodies prepared from BP patients (15, 17). However, these autoantibodies were poly-

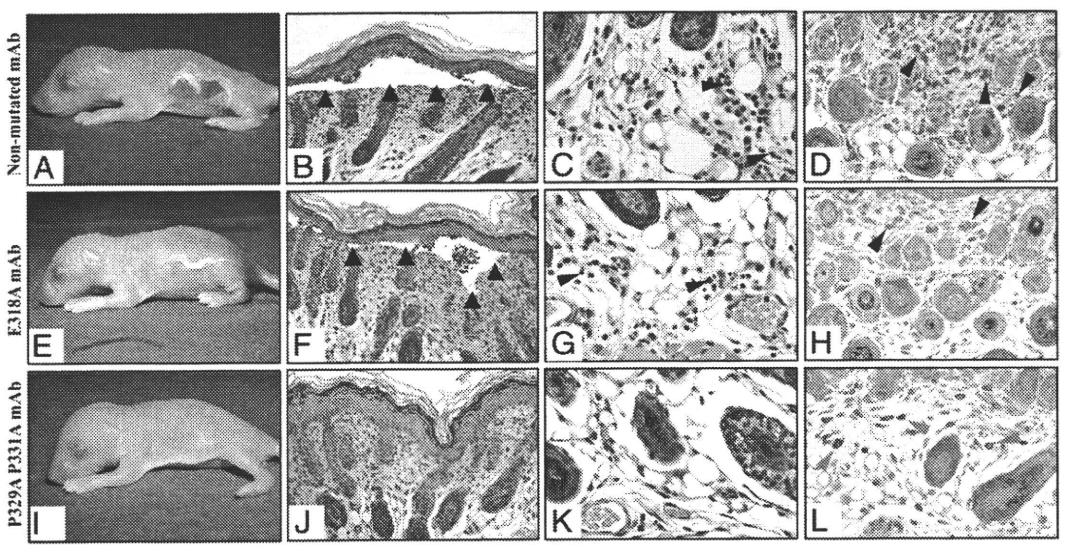

FIGURE 7. Pathogenic activity in vivo of the nonmutated and mutated IgG1 mAbs. The neonatal COL17-humanized ($COL17^{m-/-,\ h+}$) mice were i.p. injected with the nonmutated IgG1 mAb (200 μg/g body weight) or the mutated IgG1 mAbs E318A and P329A P331A (200 μg/g body weight). Forty-eight h later, pathogenic activity was determined by skin blistering test and histology biopsy of back skin including H&E and toluidine blue staining. Skin blistering is positive for the nonmutated and E318A mAbs models (*A*, *E*) and negative for the P329A P331A model (*I*). H&E staining shows epidermal detachment (black arrowheads) at the DEJ in the nonmutated (*B*) and E318A (*F*) mAbs models but not in the P329A P331A model (*J*). The numbers of neutrophils (black arrowheads) and degranulated mast cells (black arrowheads) infiltrating the dermis are more greatly reduced in the P329A P331A (*K*, *L*) model than in the nonmutated (*C*, *D*) and E318A (*G*, *H*) models. Red arrowheads indicate normal undegranulated mast cells. Original magnification ×100 (*B*, *F*, *J*); ×200 (*D*, *H*, *L*); ×400 (*C*, *G*, *K*).

Table III. *Pathogenic activity of the non-mutated and mutated IgG1 mAbs against hCO17 NC16A in the COL17-humanized* ($COL17^{m-/-,h+}$) *BP mouse model*

Abs	Mice with Skin Detachment[a], for Each Injection Dosage (μg/g Body Weight)			
	200 μg	100 μg	50 μg	25 μg
Nonmutated	8/9	5/7	4/7	0/5
Mutated				
E318A	4/6	2/5	0/5	0/4
K322A	5/8	2/6	1/6	1/5
E318A K320A K322A	3/7	2/6	0/5	0/5
P329A	1/7	1/5	0/4	0/5
P331A	1/8	0/7	0/6	0/5
P329A P331A	0/8	0/5	0/4	0/6
Normal human[b]	0/6	—	—	—

[a]Skin blistering test performed at 48 h in neonatal mice.
[b]Human IgG purified from serum in single normal volunteer.

clonal IgG containing all four IgG subclasses. In this study, we have directly demonstrated that anti-hCOL17 NC16A IgG1 mAb has pathogenic activity in vivo by using COL17-humanized ($COL17^{m-/-,h+}$) BP model mice. As previous clinical studies on BP (5, 7, 28), our results further support the notion that IgG1 autoantibodies against hCO17 are potent and possibly the main pathogenic IgG autoantibodies in BP.

Previous studies have demonstrated that activation of the complement pathway is a pivotal step in the BP pathomechanism (17, 18, 42). By comparing nonmutated and/or mutated IgG1 mAbs in terms of pathogenic activity, we have precisely analyzed the roles of C1q-binding residues of the IgG1 Fc region (E318, K320, K322, P329, and P331) in initiating complement activation both in vitro and in vivo. These results are consistent with previous mutagenesis studies that showed that these binding residues are required for complement activation in vitro (22, 25, 27). The alanine substitution at these five single-residue sites variously decreased the CDC activity of the IgG1 mAb against hCOL17 NC16A. The IgG1 mAb that was mutated at P331 showed low CDC activity in vitro, and it failed to produce a BP phenotype in the COL17-humanized ($COL17^{m-/-,h+}$) mice. In contrast, the IgG1 mAbs mutated at K322 or at E318 K320 K322 showed moderate CDC activity in vitro and high (K322) to moderate (E318 K320 K322) pathogenic activity in vivo. The other mutated mAbs (E318A and K320A), which showed high CDC activity in vitro, showed high pathogenic activity in vivo. The results of in vivo pathogenic activity and in vitro CDC and ADCC activities are summarized in Supplemental Table III. The findings suggest that the moderate CDC activity of mutated mAbs is sufficient to induce skin detachment in neonatal COL17-humanized mice and that the P331 residue is the key residue for complement activation and is required for the pathogenic activity of IgG1 mAb in vivo. Thus, complement activation ability seems to correlate with the pathogenic effects of the mutated IgG1 mAbs in COL17-humanized mice (Fig. 5, Table III). Taken together, these findings further suggest that IgG1 Fc-dependent complement activation plays a major pathogenic role in subepidermal blister formation in BP.

In the classical complement pathway, C1q binding to IgG1 triggers proteolytic cascades, which result in the generation of a large amount of C3b. This explains why the immunofluorescence intensity of mouse C1q was weaker than that of mouse C3 in DIF examinations of mouse models, as shown in Fig. 8. In addition to C3b being capable of generating membrane attack complexes as the opsonin, it induces various inflammatory reactions by binding to the complement receptors expressed on the effector cells, such as granulocytes, monocytes, neutrophils, or mast cells (43–45). In our BP mouse model, inflammatory cells, such as mast cells, neutrophils, and lymphocytes, are observed at the dermis. It has been demonstrated that C3 binding to complement receptors stimulates activation and chemotaxis of neutrophils and/or mast cells (46). Mast cells can produce various mediators, such as leukotrienes, platelet-activating factor, and cytokines, that contribute directly or indirectly to neutrophil recruitment (47, 48). The neutrophils recruited into skin then releases elastase and gelatinase B, damaging the BMZ (49, 50). These data suggest that subepidermal blistering is mediated by a complement-dependent cellular (mast-cell and neutrophil) cytotoxicity pathway.

In addition to IgG1 Abs activating complement cascades, they may directly recruit and activate effector cells via the interaction between the Fc region and reciprocal FcγRs. In this study, we analyzed the Fc-FcγR–mediated ADCC activity of IgG1 mAbs. That activity was fully defective in the IgG1 mAb that was mutated at P329, and the mutation at P331 moderately reduced the activity of the IgG1 mAb (Fig. 6). In contrast, the other mutated mAbs (E318A, K320A, K322A, and E318A K320A K322A)

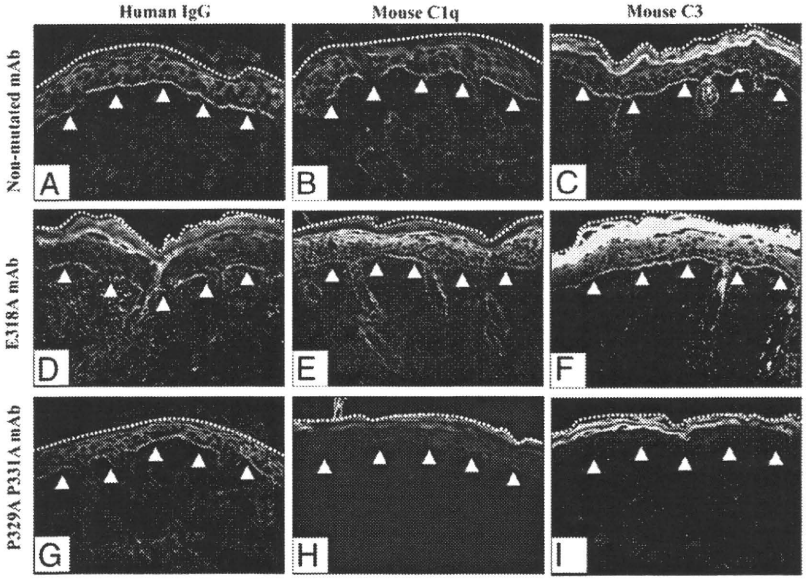

FIGURE 8. Capability of activating complement in vivo for the non-mutated and mutated IgG1 mAbs. In these three models (Fig. 7), 48 h after injection of the IgG1 mAbs, the complement activation capability was determined by DIF of human IgG and mouse complement components C1q and C3. All three of the mAbs (nonmutated IgG1, mutated E318A, and mutated P329A P331A) deposit at the DEJ (white arrowheads) (skin surface, white dotted line) of mouse skin (*A*, *D*, *G*). Mouse complement components C1q and C3 (green, FITC) are activated by the nonmutated (*B*, *C*) and E318A mAbs (*E*, *F*) but not by P329A P331A (*H*, *I*) at the DEJ (white arrowheads). Original magnification ×200 (*A–I*).

showed similar ADCC activity to that of the nonmutated IgG1 mAb. These results indicate that P329 is a key residue in IgG1-dependent ADCC reaction and that P331 plays a minor role in that process. A site-directed mutagenesis study also demonstrated that alanine substitution at the P329 residue causes the dual deficiencies of ADCC and CDC activity in vitro (25). If we focus on the pathogenic activity of IgG1 mAbs in BP, our mutagenesis studies suggest that Fc-FcγR–mediated ADCC activity may have contributed to the blister formation. In this study, in vitro CDC analysis showed that P329A and K322A had similarly moderate CDC activity (Fig. 5) but mutually distinct ADCC activity (Fig. 6). K322A showed normal ADCC activity, and P329A was incapable of triggering the ADCC reaction. Our in vivo results showed almost no skin detachment for the P329A-mutated mAb (one of seven mice) but some skin detachment for the K322A mAb (five of eight mice) (Table III). These results suggest that the ADCC (FcγR-dependent immune reaction) plays a minor but augmenting role in IgG1-dependent blister formation. This concept is further supported by a previous report by Mihai et al. (41) in which the pathogenicity of BP IgG1 and IgG4 autoantibodies was amplified by the additional recruitment of neutrophils and mast cells via Fc–FcγR interaction.

Recently, our group has used a phage display technique to develop a monoclonal Fab Ab against hCOL17 NC16A from BP patients (51). The monoclonal Fab Ab lacked pathogenic activity when administrated to neonatal COL17-humanized ($COL17^{m-/-,\ h+}$) mice. Furthermore, the monoclonal Fab Ab competitively protected the COL17-humanized ($COL17^{m-/-,\ h+}$) mice from the blister formation that would normally be induced by IgG autoantibodies prepared from BP patients. These results are consistent with our current study, and they further suggest the crucial role of the IgG1 Fc region in BP pathomechanism. In addition, complete IgG1 Ab has a longer half-life than Fab Ab in vivo (52, 53). Therefore, our current study raises the possibility that complete IgG1 mAbs with mutation at the C1q binding sites of the Fc region would protect the pathogenic epitopes from attack by the autoantibodies not only in BP but also in other autoimmune diseases in which complement activation plays an essential role.

In conclusion, to our knowledge, this study is the first in vivo evidence that IgG1 Abs targeting hCOL17 NC16A alone can trigger blister formation, and it suggests that IgG1-dependent complement activation via IgG1 Fc–C1q interaction plays a crucial role in BP.

Acknowledgments

We thank Drs. Yasuyuki Fujita, Yasuki Tateishi, and Daichi Hoshina (Hokkaido University Graduate School of Medicine) for kind discussion and technical assistance. We also thank Noriko Ikeda, Yui Kashima, Mika Tanabe, Yuko Hayakawa, and Akari Nagasaki (Hokkaido University Graduate School of Medicine) for technical assistance; Drs. Daisuke Inokuma (Hokkaido University Hospital, Sapporo), Yuka Oguchi, and Kazuo Kodama (JR Sapporo Hospital, Sapporo) for providing BP patient blood; and Dr. Kim B. Yancey for providing hCOL17 cDNA (University of Texas Southwestern Medical Center, Dallas, TX).

Disclosures

The authors have no financial conflicts of interest.

References

1. Gudi, V. S., M. I. White, N. Cruickshank, R. Herriot, S. L. Edwards, F. Nimmo, and A. D. Ormerod. 2005. Annual incidence and mortality of bullous pemphigoid in the Grampian Region of North-east Scotland. *Br. J. Dermatol.* 153: 424–427.
2. Langan, S. M., L. Smeeth, R. Hubbard, K. M. Fleming, C. J. Smith, and J. West. 2008. Bullous pemphigoid and pemphigus vulgaris—incidence and mortality in the UK: population based cohort study. *BMJ* 337: a180.
3. Jordon, R. E., E. H. Beutner, E. Witebsky, G. Blumental, W. L. Hale, and W. F. Lever. 1967. Basement zone antibodies in bullous pemphigoid. *J. Am. Med. Assoc.* 200: 751–756.
4. Nishie, W., D. Sawamura, K. Natsuga, S. Shinkuma, M. Goto, A. Shibaki, H. Ujiie, E. Olasz, K. B. Yancey, and H. Shimizu. 2009. A novel humanized neonatal autoimmune blistering skin disease model induced by maternally transferred antibodies. *J. Immunol.* 183: 4088–4093.
5. Bernard, P., P. Aucouturier, F. Denis, and J. M. Bonnetblanc. 1990. Immunoblot analysis of IgG subclasses of circulating antibodies in bullous pemphigoid. *Clin. Immunol. Immunopathol.* 54: 484–494.
6. Hofmann, S., S. Thoma-Uszynski, T. Hunziker, P. Bernard, C. Koebnick, A. Stauber, G. Schuler, L. Borradori, and M. Hertl. 2002. Severity and phenotype of bullous pemphigoid relate to autoantibody profile against the NH_2- and COOH-terminal regions of the BP180 ectodomain. *J. Invest. Dermatol.* 119: 1065–1073.
7. Laffitte, E., M. Skaria, F. Jaunin, K. Tamm, J. H. Saurat, B. Favre, and L. Borradori. 2001. Autoantibodies to the extracellular and intracellular domain of bullous pemphigoid 180, the putative key autoantigen in bullous pemphigoid, belong predominantly to the IgG1 and IgG4 subclasses. *Br. J. Dermatol.* 144: 760–768.
8. Stanley, J. R., P. Hawley-Nelson, S. H. Yuspa, E. M. Shevach, and S. I. Katz. 1981. Characterization of bullous pemphigoid antigen: a unique basement membrane protein of stratified squamous epithelia. *Cell* 24: 897–903.
9. Sitaru, C., E. Schmidt, S. Petermann, L. S. Munteanu, E. B. Bröcker, and D. Zillikens. 2002. Autoantibodies to bullous pemphigoid antigen 180 induce dermal-epidermal separation in cryosections of human skin. *J. Invest. Dermatol.* 118: 664–671.
10. Giudice, G. J., D. J. Emery, B. D. Zelickson, G. J. Anhalt, Z. Liu, and L. A. Diaz. 1993. Bullous pemphigoid and herpes gestationis autoantibodies recognize a common non-collagenous site on the BP180 ectodomain. *J. Immunol.* 151: 5742–5750.
11. Anhalt, G. J., C. F. Bahn, R. S. Labib, J. J. Voorhees, A. Sugar, and L. A. Diaz. 1981. Pathogenic effects of bullous pemphigoid autoantibodies on rabbit corneal epithelium. *J. Clin. Invest.* 68: 1097–1101.
12. Liu, Z., L. A. Diaz, J. L. Troy, A. F. Taylor, D. J. Emery, J. A. Fairley, and G. J. Giudice. 1993. A passive transfer model of the organ-specific autoimmune disease, bullous pemphigoid, using antibodies generated against the hemidesmosomal antigen, BP180. *J. Clin. Invest.* 92: 2480–2488.
13. Oikarinen, A. I., J. J. Zone, A. R. Ahmed, U. Kiistala, and J. Uitto. 1983. Demonstration of collagenase and elastase activities in the blister fluids from bullous skin diseases: comparison between dermatitis herpetiformis and bullous pemphigoid. *J. Invest. Dermatol.* 81: 261–266.
14. Ståhle-Bäckdahl, M., M. Inoue, G. J. Guidice, and W. C. Parks. 1994. 92-kD Gelatinase is produced by eosinophils at the site of blister formation in bullous pemphigoid and cleaves the extracellular domain of recombinant 180-kD bullous pemphigoid autoantigen. *J. Clin. Invest.* 93: 2022–2030.
15. Liu, Z., W. Sui, M. Zhao, Z. Li, N. Li, R. Thresher, G. J. Giudice, J. A. Fairley, C. Sitaru, D. Zillikens, et al. 2008. Subepidermal blistering induced by human autoantibodies to BP180 requires innate immune players in a humanized bullous pemphigoid mouse model. *J. Autoimmun.* 31: 331–338.
16. Chen, R., G. Ning, M. L. Zhao, M. G. Fleming, L. A. Diaz, Z. Werb, and Z. Liu. 2001. Mast cells play a key role in neutrophil recruitment in experimental bullous pemphigoid. *J. Clin. Invest.* 108: 1151–1158.
17. Nishie, W., D. Sawamura, M. Goto, K. Ito, A. Shibaki, J. R. McMillan, K. Sakai, H. Nakamura, E. Olasz, K. B. Yancey, et al. 2007. Humanization of autoantigen. *Nat. Med.* 13: 378–383.
18. Nelson, K. C., M. Zhao, P. R. Schroeder, N. Li, R. A. Wetsel, L. A. Diaz, and Z. Liu. 2006. Role of different pathways of the complement cascade in experimental bullous pemphigoid. *J. Clin. Invest.* 116: 2892–2900.
19. Jordon, R. E., S. Kawana, and K. A. Fritz. 1985. Immunopathologic mechanisms in pemphigus and bullous pemphigoid. *J. Invest. Dermatol.* 85(Suppl. 1)72s–78s.
20. Provost, T. T., and T. B. Tomasi, Jr. 1973. Evidence for complement activation via the alternate pathway in skin diseases. I. Herpes gestationis, systemic lupus erythematosus, and bullous pemphigoid. *J. Clin. Invest.* 52: 1779–1787.
21. Jordon, R. E., N. K. Day, W. M. Sams, Jr., and R. A. Good. 1973. The complement system in bullous pemphigoid. I. Complement and component levels in sera and blister fluids. *J. Clin. Invest.* 52: 1207–1214.
22. Duncan, A. R., and G. Winter. 1988. The binding site for C1q on IgG. *Nature* 332: 738–740.
23. Burton, D. R. 1985. Immunoglobulin G: functional sites. *Mol. Immunol.* 22: 161–206.
24. Oganesyan, V., C. Gao, L. Shirinian, H. Wu, and W. F. Dall'Acqua. 2008. Structural characterization of a human Fc fragment engineered for lack of effector functions. *Acta Crystallogr. D Biol. Crystallogr.* 64: 700–704.
25. Idusogie, E. E., L. G. Presta, H. Gazzano-Santoro, K. Totpal, P. Y. Wong, M. Ultsch, Y. G. Meng, and M. G. Mulkerrin. 2000. Mapping of the C1q binding site on rituxan, a chimeric antibody with a human IgG1 Fc. *J. Immunol.* 164: 4178–4184.
26. Tao, M. H., R. I. Smith, and S. L. Morrison. 1993. Structural features of human immunoglobulin G that determine isotype-specific differences in complement activation. *J. Exp. Med.* 178: 661–667.
27. Xu, Y., R. Oomen, and M. H. Klein. 1994. Residue at position 331 in the IgG1 and IgG4 C_H2 domains contributes to their differential ability to bind and activate complement. *J. Biol. Chem.* 269: 3469–3474.
28. Döpp, R., E. Schmidt, I. Chimanovitch, M. Leverkus, E. B. Bröcker, and D. Zillikens. 2000. IgG4 and IgE are the major immunoglobulins targeting the